Raja, Wasif Rehman

Quantitative Seismic Geomorphology of Cenozoic submarine channel system in the Canterbury Basin, Offshore New Zealand: Implications for paleoenvironment interpretation and hydrocarbon prospectivity

July 2019

Master's thesis

2019

Master's thesis

Raja, Wasif Rehman

NTNU
Norwegian University of
Science and Technology

NTNU
Norwegian University of
Science and Technology

NTNU

Norwegian University of
Science and Technology

Quantitative Seismic Geomorphology of Cenozoic submarine channel system in the Canterbury Basin, Offshore New Zealand: Implications for paleoenvironment interpretation and hydrocarbon prospectivity

Raja, Wasif Rehman

This thesis is dedicated to my parents, brother, sisters, and my family.

Acknowledgment

Abstract

Nowadays, high resolution 3D marine seismic reflection data have allowed to study the morphology of submarine channels (primary conduits to transfer sediment from shelf to the basin) to understand the sedimentary processes and paleoenvironments. However, the interpretation of channels incision or channel isolated amplitude (related to the seismic reflection data resolution) from the 3D marine seismic reflection data poses several challenges due to the presence of data artifacts (e.g. velocity push-downs issues in the study area). The quantitative seismic geomorphology approach, together with traditional seismic interpretation (e.g. interpretation of horizon and fault followed by seismic slicing and seismic attribute analysis) are used in this study to obtain the 3D channels morphometric elements. In addition, regional correlation that utilized 2D seismic reflection and wellbore data providing regional stratigraphy and tectonic information. This study aim to describe architecture and morphometry elements of submarine channels in the Canterbury basin, offshore New Zealand. Thus, sedimentary processes, and paleoenvironment of submarine channel systems in the study area is much more understandable and implication to the hydrocarbon prospectivity could also be described. Submarine channels morphometric parameters such as thalweg (the lowest point of channel base), height, top and base widths, sinuosity, gradient (thalweg), aspect ratio (width/height), and cross-sectional area (CSA) and the relationships among them are measured at an interval of 150-meter perpendicular to the pathways of the channels. Four types of submarine channels are found in the study area based on reflection configuration of channels fills, shape of erosional surfaces, stacking patterns and architectural elements. Furthermore, this thesis work show that channels top width and height vary from proximal to distal part in the context of hundred to thousand meters, respectively. These indicated combination of submarine gravity flow and internal factors (e.g. over-bank collapse, tributaries, etc) in the development of submarine channels system in the study area. In addition, submarine channel system in the study area is also having potential in generating and preserving hydrocarbon.

Table of Contents

List of Tables

List of Figures

Chapter 1

Introduction

1.1 Background of study

The Submarine channel is primary conduits to transfer sediment from shelf to the basin floor area and when they are filled with sand or silt type deposits in deep water basin they become good hydrocarbon reservoirs (Mutti and Normark, 1991; Mayall and Stewart, 2000; Mayall et al., 2006; Wynn et al., 2007).

Submarine channels are more common in distal slope regions where erosional and aggradational processes combine together to form meandering systems (Mayall et al., 2006; Abreu et al., 2003; Deptuck et al., 2003; McHargue et al., 2011). Nevertheless, both features are related, as submarine channels are usually developed within and at the lower reaches of submarine canyons (Wynn et al., 2007; Shepard, 1965), sharing strong analogies with sub-aerial river systems (Kolla et al., 2001; Clark et al., 1992; Posamentier, 2006; Straub et al., 2012). The genesis and evolution of submarine channels depend on basin tectonics, climate, and sea-level changes, factors that control the type, supply and deposition of sediment (Kolla, 2007; Bouma, 2004).

The recent advancement in marine geophysical data enables to organize and compare architectural elements associated with a submarine channel (Clark and Pickering, 1996; Deptuck et al., 2007; Qin, 2017; Mutti and Normark, 1987; Jobe et al., 2011). In addition, high resolution 3D marine seismic reflection data have allowed to study the morphology of submarine channels to understand the sedimentary processes and paleoenvironments (Harishidayat et al., 2018; Qin, 2017). However, the interpretation of channels incision or channel isolated amplitude (related to the seismic reflection data resolution) from the 3D marine reflection data poses several challenges due to the presence of data artifacts (e.g. velocity push-downs issues in the study area). Moreover, the quantitative seismic geomorphology approach, together with traditional seismic interpretation (seismic facies analysis, attribute analysis and slicing) are used in this study to obtain the 3D channels morphomet-

ric elements, since the quantification of channel morphological and spatial data is relevant to understand the organization of both submarine or sub-aerial channel systems and their controlling factors (Hajek et al., 2010; Hofmann et al., 2011). In addition, the implication for hydrocarbon prospectivity will also be achievable.

The study area is located in the South Western part of the Canterbury basin (Figure 2.1) that includes the Waka 3D Seismic reflection data and Caravel-1 wellbore data. Previous study documented that the Channel initiation is to be Early Oligocene to Miocene time when the deep-marine environment occurred (Sahoo et al., 2015; Zhao et al., 2016). However, documentation and description of the deep-marine channel system in the study area are very limited. Thus, the sedimentary process, detail paleoenvironment and hydrocarbon implications in the study area are poorly understood.

1.2 Aims of this study

The aims and objectives of this thesis are as follows:

1. Describe seismic architectures and depositional elements of several types of submarine channels.

2. Describe their morphometric elements and scaling relationship among them.

3. Investigate the sedimentary processes and paleoenvironment of submarine channels.

4. Investigate the study implications for hydrocarbon prospectivity in the study area.

1.3 Thesis structure

The thesis is structured as follows:

- Chapter 1: Introduction which comprises the background, aim and thesis structure.

- Chapter 2: Geological settings that include the setting of New Zealand and the Canterbury Basin.

- Chapter 3: Overview of submarine channels systems as a literature study on the current understanding of the architectural elements and geomorphology of the submarine channel and channel complexes.

- Chapter 4: Data and methodology which include the availability of data for thesis work and methodologies used to reveal the objective of the study.

- Chapter 5: Presentation of the results of this study. Firstly, the qualitative results include well to seismic tie, horizon and faults interpretation, slicing methods, incision interpretation, seismic facies analysis and then the quantitative results that include the mapping and morphometric parameter calculations of submarine channels.

- Chapter 6: Discussion of the results given in Chapter 5 that include the sedimentary processes and paleoenvironment interpretation. Thus, hydrocarbon prospectivity will be achievable. In addition, morphometry comparison with other sediment conduits is also discussed.

- Chapter 7: Conclusion of the thesis work.

Chapter 2

Geological Setting

2.1 New Zealand Geology

The geology of New Zealand is noted for its volcanic activity, earthquakes and geothermal areas because of its position on the boundary of the Australian Plate and Pacific Plates. New Zealand is part of Zealandia, a microcontinent nearly half the size of Australia that broke away from the Gondwanan supercontinent about 83 million years ago (Wallis and Trewick, 2009). New Zealand is a fragment of Gondwana that, before Late Cretaceous seafloor spreading, was contiguous with Australia and Antarctica. Only about 10% of the area of continental crust in the wider New Zealand region (Zealandia) is emergent above sea level as the North and South Islands (Figure 2.1). In addition, no Precambrian cratonic core is exposed to onland New Zealand (Mortimer, 2004).

New Zealand is submerged because of tectonic subsidence caused by Cretaceous-Paleogene rifting, not the global rise of sea level. Paleozoic and Mesozoic rocks of New Zealand were forged by inter-plate processes on the margin of Gondwanaland, around (510-110 Ma) during the Cambrian to the Cretaceous period (Campbell et al., 2012). A profound tectonic change occurred in the earliest Miocene, although the beginnings may be traced to the Eocene in the far North and South of New Zealand. Movement at the modern-day active plate boundary was very slow during the Eocene and Oligocene time in New Zealand, but rapidly accelerated at the beginning of the Miocene (Cande and Stock, 2004). The current emergent parts of the New Zealand continental crust block has been lifted above sea level by collisional tectonism and associated crustal thickening beginning in the late Oligocene or early Miocene (Cooper et al., 1987). Present day New Zealand is the exposed part of a largely submerged continent named: Zealandia. This has been confirmed by rock sampling (dredged samples from the seafloor) and geophysical exploration, as explained by (Mortimer and Campbell, 2014).

Figure 2.1: Spatial limits of Zealandia. Base map modified after Trewick et al. (2007). Red highlighted shape represent Canterbury basin location & white box represent the study area with wellbore locations.

Zealandia includes the Campbell Plateau to the South of New Zealand, the Challenger Plateau to the West, the Chatham Rise to the East, and the Lord Howe Rise to the Northwest, and Norfolk Ridge to the North (Figure 2.1). The Lord Howe Rise, Challenger Plateau and Norfolk Ridge to the northwest of New Zealand (Figure 2.1) and comprise

continental crust situated on the Australian Plate, whereas the Chatham Rise and Campbell Plateau to the east and southeast of New Zealand are pieces of continental crust located on the Pacific Plate. In Geological point, about (25 Ma to present) New Zealand has risen from the sea that's why it is predominantly tectonic rather than the volcanic origin and effectively an oceanic archipelago, although it comprising continental crust (Trewick et al., 2007). This configuration of land and sea and the boundary between the two plates is relatively recent in the long history of New Zealand's evolution. The present plate boundary probably attained its position only about 10 Ma ago (Gaina et al., 1998).

The study area is located in the western part of the Bounty Trough; Canterbury basin that resides in an area of active earth deformation, as a result of the oblique continental collision of the Australian and Pacific plates along the Alpine Fault to the west of the region (Stirling et al., 2001). Furthermore, the upper crustal structure of the northern Canterbury basin is dominated by north and northeast-trending faults and the folds formed to accommodate plate motion between the Hikurangi plateau and the Alpine Fault (Figure 2.1), whereas the central and south Canterbury regions dominated by north trending active structures as a response to deformation from continent collision of the Southern Alps (Pettinga et al., 2001).

2.2 Geological Setting of The Canterbury Basin

2.2.1 Mid-Cretaceous Rifting

The Creation of the Canterbury basin was initiated during the Cretaceous due to the breakup of eastern Gondwana (Browne and Field, 1988). Prior to the breakup of Gondwana, the Australian margin was a convergent plate boundary (Figure 2.2) with the Phoenix plate being subducted westward along with an extensive trench system (Ballance, 1992). Normal faulting was responsible for creating the primary basin architecture and due to this a series of fault angle depression created but, these half grabens subsided rapidly and locally filled with non marine to paralic deposits, However, local tectonism and regional (thermally driven) subsidence continued through Cretaceous producing transgression and onlap of terrestrially derived sediments (O'Leary and Mogg, 2008).

The rifting episode was associated with the final separation of New Zealand, Antarctica, and Australia during Gondwanaland break-up (Browne and Field, 1988; Cook et al., 1999; Carter, 1988) and these synrift fault systems are pronounced in the entire study area except the northwestern region (Sahoo et al., 2015). In addition, sediments deposited in the syn-rift phase range in age from the mid Cretaceous (Davey et al., 1982) to the middle part of the Late Cretaceous (O'Leary and Mogg, 2008) therefore, the terrestrial conglomerate, sandstone, siltstone, carbonaceous mudstone, and coal (Figure 2.3) were deposited in grabens (Sutherland and Browne, 2003).
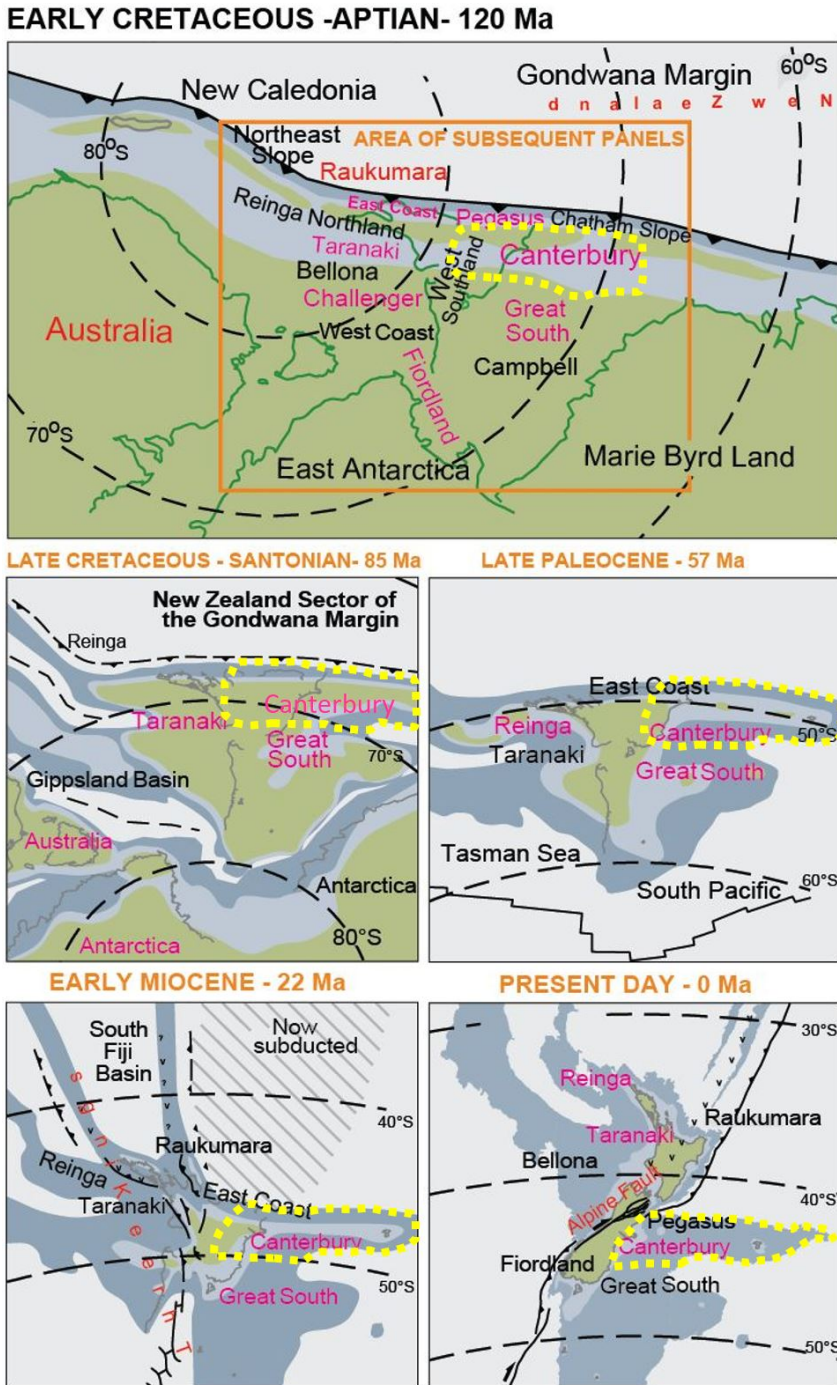
Figure 2.2: Paleogeographic Maps modified after King (2000), and Uruski (2010), encircle yellow color represents Canterbury basin location.

2.2.2   Late Cretaceous to Oligocene passive Margin

During this time the Canterbury basin was largely tectonically inactive and overall marine transgression occurred during thermal subsidence (Sahoo et al., 2015). Passive subsidence followed rifting, resulting in transgression towards the northwest, and the Passive subsidence continued during Paleogene time (Sutherland, 1995). This resulted in a first-order fining-upward sequence until the entire sequence was cover completely by mudstone (Figure 2.3). The development of volcanism is observed in the clipper sub-basin (Figure 2.1) and is probably associated with the creation of oceanic crust between Antarctica and Australia during the Paleocene time (Todd, 1984). The organic-rich black shales were deposited in Late Paleocene time, followed by an increase in carbonate content during Eocene time in the basin, whereas at late Eocene time a new plate boundary propagated into New Zealand (Sutherland, 1995), but the Canterbury basin was outside the deformed region and continued to passively subside, and due to this a layer of outer neritic mudstone and micrite was deposited in Eocene time. Bathyal micritic limestone in the early Oligocene is separated from late Oligocene packstone and grainstone by the Marshall paraconformity (Browne and Field, 1988) and Transgression reached at its peak in Oligocene time, when widespread limestones were deposited (Browne and Field, 1988; Cook et al., 1999; Carter, 1988).

2.2.3   Miocene to Recent transcurrent tectonics

Late Oligocene to Recent deposition reflects progressive uplift and erosion of Southern Alps, with resulting marine regression (Browne and Field, 1988). An influx of terrigenous sediment from the west combined with strong oceanic currents produced a stacked sequence of rapidly prograding sediment drift prisms (Fulthorpe et al., 1996). After that, the Coarse clastic terrestrial and shallow marine sediments were deposited in the west and localized coarse-grained carbonates in the north. In eastern parts of the basin, distant from rising mountain ranges, fine-grained sediments continued to be deposited. In northwestern parts of the basin, faults have been reactivated and anticlines have grown in response to transpressive plate motion (Sutherland and Browne, 2003). The drift of the Pacific plate's pole (Figure 2.2) of rotation has increased the amount of oblique convergence across the Alpine Fault (Walcott, 1979). Erosion of the rapidly uplifting southern Alps provided sediment to the Canterbury shelf which continued to prograde throughout the Plio-Pleistocene (Browne and Field, 1988) resulting in a 2200 meter thick sequence of eastward fining interbedded conglomerates (alluvial fans), silt, shelf beds, and clay (Figure 2.3). During the last 5 million years, rapid uplift and erosion of the Southern Alps have greatly increased the supply of coarse clastic sediment. In northwestern parts of the basin, faults have been reactivated and anticlines have grown in response to transpressive plate motion, whereas the Intraplate volcanism is known to have occurred intermittently and locally from Late Cretaceous to Pliocene time, with no apparent pattern emerging (Browne and Field, 1988).
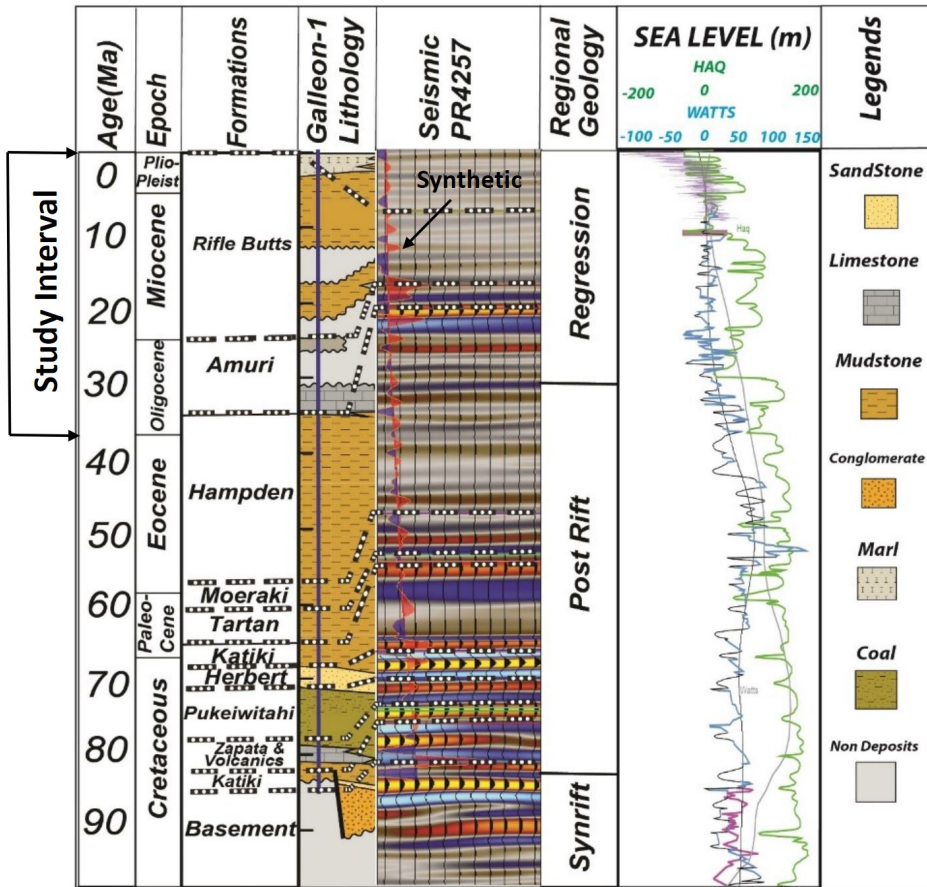
Figure 2.3: Stratigraphic column of the study area in the Canterbury basin modified after Petroleum (2014) together with Seismic Well-Tie of Galleon-1 and sea level curve of Miller et al. (2005). See Figure 2.1 for wellbore location.

Chapter 3

Overview of submarine channels system

3.1 Architectural Elements

"In order to build a conceptual framework for comparing modern and ancient turbidite systems Mutti and Normark (1987) introduced the concept of the element, which includes channels, overbank deposits, lobes, channel/lobe transition features, and scours, to provide a characterization of facies assemblage. The term architectural element was later borrowed from fluvial system to build a hierarchical classification of depositional elements in turbidite system (Miall, 1989). An architectural element is a depositional body defined by its geometry, scale, and facies (Miall, 1989; Pickering et al., 1995). It is formed by a particular process or series of processes within a depositional system (Miall, 1989)". The architectural elements associated with submarine channel systems such as channel belt, thalweg deposits, basal lags, bank failures, levees, channel fills and deposits associated with lateral channel migration have been documented in earlier research " (e.g. Mutti and Normark, 1991; McHargue and E. Webb, 1986; Mutti and Ricci Lucchi, 1978; Shanmugam and Moiola, 1988)".

3.1.1 Channel belt

The region occupied by channel fills or channel fill complexes is commonly referred to as a channel belt, and it is the combination of internal levees, depositional terraces and slide blocks of external levee sediment make up thin-bedded turbidites within channel belt (Figure 3.1) whereas, In the case of depositional terraces the space available in the channel belt is insufficient for the current to decelerate and deposit the majority of its sediment before reaching the bounding topography of the channel belt, creating confined sheet-like

deposits (Hansen et al., 2017). The depositional sites for internal levees and depositional terraces within channel belts can be formed by various processes such as entrenchment, point bar accretion, meander bend cut-off, channel margin failure, or changes in the flow parameters. However, the development and preservation of levees and terraces are closely related to the evolution of the channel belt as a whole, which is controlled both by allogenic and by autogenic mechanisms (Gamberi et al., 2013).

3.1.2 Thalweg deposits

Channel floors are often incised by a relatively narrow inner channel called the thalweg, while coarse-grained deposits such as spillover lobes and crevasse splays have been observed on outer bend levees (Figure 3.1). However, it is not clear that these are coarse-grained as equivalent channel thalweg deposits, nor that outer bend channel levees generally are as coarse-grained as channel deposits (Wynn et al., 2007). Stability of the channel pattern, as well as stability of the thalweg line, can have both local and regional causes whereas, In young rivers, which flow through areas of outcropping solid rocks, the thalweg stability may result from the presence of outcrops of rocks resistant to erosion. In addition, the Stabilization of the channel and the thalweg line in mature rivers with a developed erosional base may result from the resistance of older channel alluvial series of the same river to erosion (Falkowski et al., 2018).
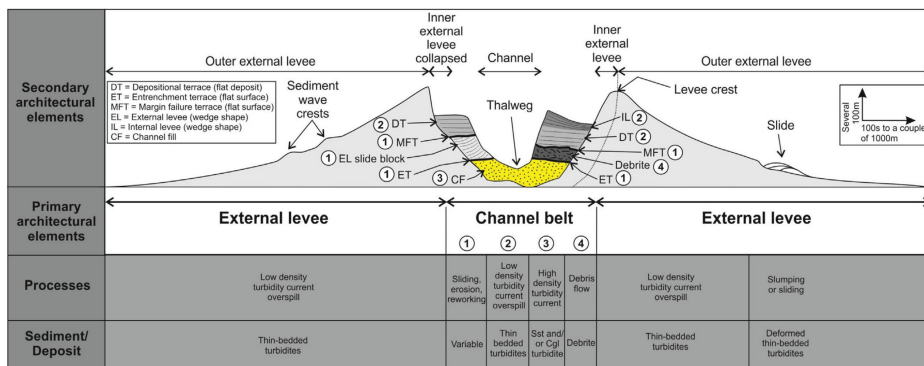
Figure 3.1: Typical channel-levee cross-section (Hansen et al., 2017).

3.1.3 Basal lags

Basal lags are deposits accumulated on the channel floor (Figure 3.1, Figure 3.2) when turbidity currents bypass channels (Normark et al., 1993). There are, at least, three types of basal-lag depositional facies recorded in the literature: 1) coarse sands and conglomerates, 2) mud-clast conglomerates, and 3) shale drapes (Mayall et al., 2006). The reservoir properties of the channel base are closely linked with these three types of basal lag deposits (Mayall et al., 2006). For example, coarse sands and conglomerates form high

permeability zones and mud-clast conglomerates and shale drapes from the permeability barriers (Mayall et al., 2006). Basal lags in channels are mostly interpreted as High Amplitude Reflections (HARs) on seismic data which are discontinuous, high amplitude seismic reflections (Damuth et al., 1983; Stelting et al., 1985).

3.1.4 Bank failures

Bank failures can be recognized by the presence of amphitheater-shaped scars on the banks of channel systems (Deptuck et al., 2003; Cronin et al., 2005). Their corresponding deposits are usually composed of a muddy matrix, and muddy to clean sands which shows a contorted internal structure (Cronin et al., 1998; Mayall et al., 2006). Furthermore, excess over-pressures are considered to be the main cause of mass failures on channel margins. These over-pressures are often generated during the rapid deposition of low-permeability, fine-grained sediment such as levee deposits (Dugan and Sheahan, 2012; Sawyer et al., 2014). The relationship between levee height and bank failure using numerical models by Sawyer et al. (2014) show that rapid levee deposition above the channel banks can generate high fluid pressures in near-seafloor strata, reducing effective stresses within the strata and promoting mass failures above a critical bank height. In addition, local over-steepening of channel walls resulting from undercutting is another mechanism capable of causing bank failures (Deptuck et al., 2003; Catterall et al., 2010; Noda et al., 2008).

3.1.5 Levees

Levees are over-bank deposits with gull-wing geometries that converge away from the channel thalweg (Figure 3.1). External levees (outer levees sensu Deptuck et al., 2003, 2007); also the (master-bounding levees sensu Posamentier and Kolla, 2003) and internal levees (inner levee sensu Deptuck et al., 2003, 2007) are used to differentiate levees deposited outside and inside the valley (Kane and Hodgson, 2011). The levees are mostly identified on the seismic data as high to low amplitude, continuous, parallel to subparallel, and wedge-shaped reflections (Janocko et al., 2013; Kane and Hodgson, 2011). In submarine channel systems two types of scales are documented: 1) external levees (Deptuck et al., 2003, 2007) that confine submarine channel complexes; and 2) internal levees (Deptuck et al., 2003) that confine submarine channels (Kane and Hodgson, 2011).

Within submarine complexes, accommodation space for internal-levee deposition is often provided by features such as erosional terraces, abandoned meander loops and slumps or slides (Babonneau et al., 2004; Deptuck et al., 2003). On the other hand, the sediment waves have been recognised on the external levees of submarine channel systems (Nakajima et al., 1998; Wynn et al., 2007). They are symmetrical to asymmetrical wave-like bed-forms observed in unconfined submarine environments and are formed by spillover and flow stripping due to super-elevation of turbidity currents associated to centrifugal forces (Piper and Normark, 1983; Normark et al., 2002).

3.1.6 Channel fills

Channel-fill deposits are evidence for the abandonment stage (Figure 3.1) of submarine channels (Wynn et al., 2007; Janocko et al., 2013). They differ in-term of sand to mud-prone, high to low amplitude (continuous) horizontal seismic reflections (Janocko et al., 2013), and commonly show convex-upward "hat" shapes after compaction (Posamentier, 2003). The differential compaction of the axial sandy fills deposited adjacent to muddy deposits also possess similar geometrical settings (Posamentier, 2003).

3.2 Geomorphology of submarine channels and channel complexes

3.2.1 Channel dimensions

The cross-section of a channel is commonly symmetrical when the channel is relatively straight; however, it is considerably asymmetric at meander bends (Wynn et al., 2007; Kolla et al., 2001; Deptuck et al., 2007). In addition, the channel shows steeper margins on its outer bends and gentler margins on its inner bends on later stages (Figure 3.2). Submarine channels documented by literature are generally hundreds of meters wide, and tens of meters high (Shanmugam and Moiola, 1988). The morphological data from submarine and fluvial channels compiled by (Jobe et al., 2016) from a range of tectonic settings to find that the average thickness of channels and channel belts in the submarine realm is much larger than in sub-aerial settings.

3.2.2 Channel Complex dimensions

Morphological variations in the channel complexes are quite prominent as shown in (Figure 3.2) and also documented in the literature. For example, channel complexes can be less than 1000 m wide and similar to the width of submarine channels (Gardner et al., 2003; Thomas and Bodin, 2013; Macauley and Hubbard, 2013). In comparison, channel complexes wider than 3000 m have been recorded on seismic data (Deptuck et al., 2007; Catterall et al., 2010; Jolly et al., 2016), and at outcrop studies (Grecula et al., 2003). These distinct variations are likely due to differences in the degree of lateral channel migration, and by channel kinematics, influenced by local factors (Jobe et al., 2016; Bain and Hubbard, 2016).
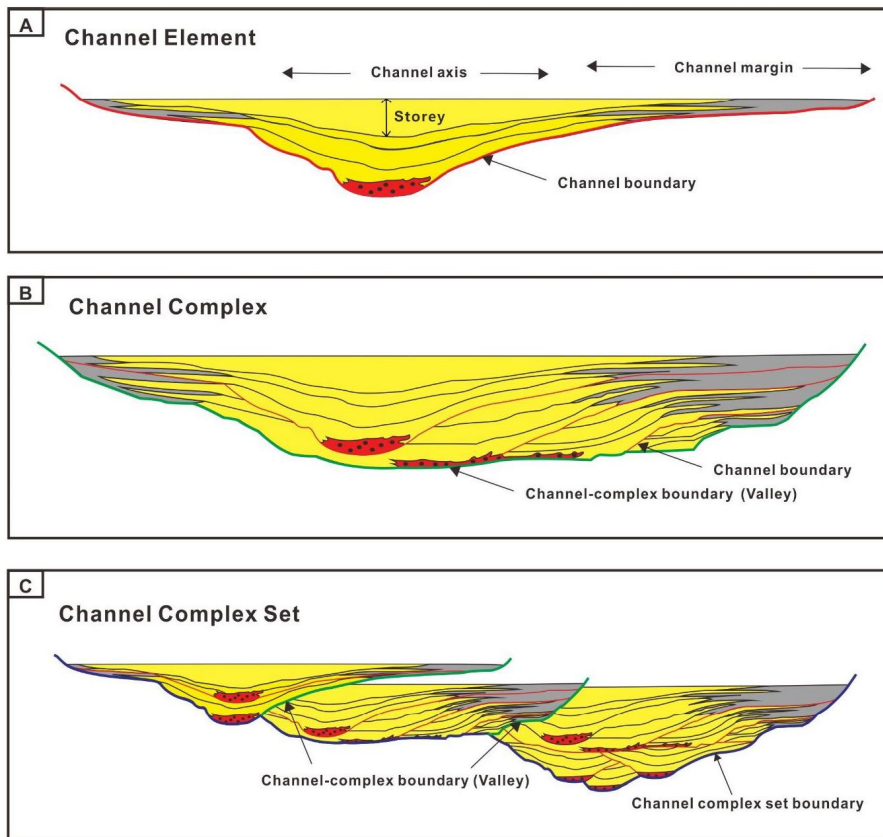
Figure 3.2: Schematic diagram showing the stratal hierarchy of submarine channels (Di Celma et al., 2011). The channel element, the channel complex, and the channel complex set are commonly observed architectural elements of this hierarchical framework. Envelope-shaped facies at the base of channel element is basal lag deposits.

3.2.3 Channel sinuosity

Sinuosity is a prominent characteristic of submarine channels and it can be formed either at an early incision stage or at subsequent aggradation stages (Mayall et al., 2006). Different type of channel sinuosity, including downstream or upstream translation, lateral expansion, or a combination of all these, have been found in submarine channels (Chough and Hesse, 1976).

The Channel sinuosity is affected by other factors such as tectonic controls and Sediment supply (grain size, density, and frequency of turbidity current) (Weimer, 1991; Babonneau et al., 2002; Clark and Pickering, 1996). For example, Babonneau et al. (2002) suggest that decreases in flow energy and erosive power down-slope result in a decrease in channel sinuosity. However, it is difficult to evaluate the relationship between sediment sup-

ply and channel sinuosity without lithological data. Additionally, some authors suggest that channel sinuosity increases with time, and the meander cut-offs forming during this process (Deptuck et al., 2003; Wynn et al., 2007; Gee et al., 2007; Maier et al., 2013). Furthermore, Gee et al. (2007) and Maier et al. (2013) proposed an evolutionary model in which submarine channels developed from relatively straight to more sinuous pathways. In addition, the flow of frequency may be important in this process as a flow of frequency increases with time within a specific channel, thus resulting in increased channel sinuosity.

Previous studies have also linked the variations of channel sinuosity to other factors such as Coriolis force (Peakall et al., 2013; Wells and Cossu, 2013). In addition, Peakall et al. (2013) found that more sinuous channels tend to be located in low latitudinal areas, while less sinuous channels tend to be located in the higher latitudinal area. Seafloor topography is another factor influencing channel pathways and associated sinuosity (Mayall et al., 2006; Clark and Cartwright, 2011).

3.3 Hierarchical framework and terminology associated with submarine channels

Previous studies have listed a number of hierarchical framework linked with submarine channels, these hierarchical framework help to classify and integrate genetically related channel to form sand bodies from various settings, locations, and data-sets (Mutti and Normark, 1987; Pickering et al., 1995; McHargue et al., 2011; Sprague et al., 2005). For example, Mutti and Normark (1987) proposed five orders of spatial and temporal scales of turbidite deposits: complex, system, stage, sub-stage and beds. Pickering et al. (1995) applied the classification of zero to sixth order bounding-surface hierarchy to the submarine environment. Some authors built hierarchical scales based on outcrop studies of submarine channels (Campion et al., 2003; Gardner and Borer, 2000).

The hierarchical framework used in this thesis is similar to the classification of Sprague et al. (2005) and McHargue et al. (2011). Three orders of stratigraphic elements, channel element, channel complex and channel complex set (Figure 3.2), all of which are extensively described and mostly used in the published literature's (Clark and Pickering, 1996; Di Celma et al., 2011; Abreu et al., 2003; Bain and Hubbard, 2016; Thomas and Bodin, 2013). The Channel element is the fundamental element of the hierarchical framework and it consists of a channel-form erosional surface and the sediments fill within the erosional surface (McHargue et al., 2011). Moreover, the term 'channel' here refers to V, and U shaped, with a morphological feature on the seafloor.

Channel complex is an architectural element of a higher order than the channel element (Figure 3.2). It is composed of two or more genetically related channel-fill episodes and is formed by lateral migration and vertical stacking of a single channel element (Abreu et al., 2003; McHargue et al., 2011; Thomas and Bodin, 2013). It refers to channel belt in some studies (Deptuck et al., 2003; Posamentier and Kolla, 2003; Catterall et al., 2010; Kane and Hodgson, 2011; Jobe et al., 2016; Hansen et al., 2015). In addition, the Channel

complex set (Figure 3.2) is composed of multiple genetically related channel complexes (McHargue et al., 2011).

3.4   Deposits associated with lateral migration

In submarine channels, two types of migration, discrete and continuous migration (Figure 3.3), have been widely documented in the literature from high-resolution subsurface data (Abreu et al., 2003; Deptuck et al., 2003, 2007). The change in the flow properties helps to interpret these migration changes (Kolla et al., 2001; Kolla, 2007). Steady and surge-type turbidity currents result in varying degrees of discrete and continuous channel migration, while steadier flows cause subtler and more continuous lateral channel migration than surge flows (Kolla et al., 2001; Kolla, 2007).
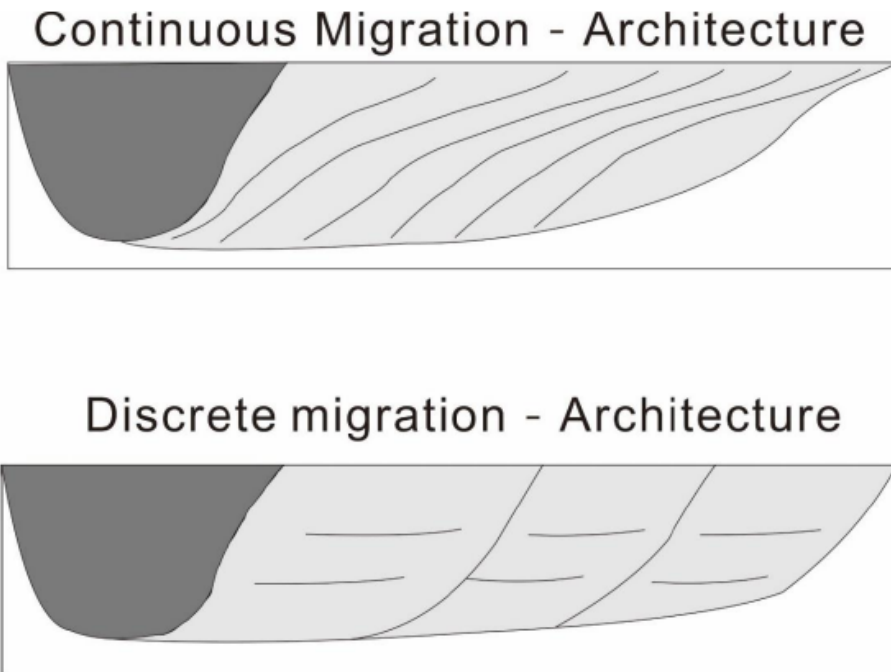
Figure 3.3: Comparison between continuous and discrete lateral migration in submarine channels (Qin, 2017). Continuous migration is characterized by inclined strata, while discrete migration is characterized by sub-horizontal strata.

3.4.1 Continuous migration

Lateral Accretion Packages (LAPs) are located at the inner bends of channels and are characterized by: a). inclined seismic reflections dipping towards the channels axis in vertical seismic profiles, and b). "scroll bar" geometries on horizon slices (Abreu et al., 2003). They represent the lateral accretion of sediments formed by lateral migration of the channel thalweg (Figure 3.4), in a process similar to the formation of point-bars in fluvial channels (Abreu et al., 2003).

Lateral-accretion deposits, which correspond to LAPs on seismic data, have been documented at outcrop (Abreu et al., 2003; Pyles et al., 2010). Lithofacies associated with these deposits range from conglomerates, coarse-sandstones to sandy and muddy turbidites (Abreu et al., 2003). Fining-upward trends (Abreu et al., 2003; Wynn et al., 2007) and coarsening-upward profiles (Pyles et al., 2012) are both found in 'point bars' of submarine channels. Two repeating and inter-stratified types of strata are documented by (Arnott, 2007) which are: a). coarse-grained deposits consisting of strata as coarse as granule conglomerates, and b). fine-grained deposits composed of thin- to medium-bedded fine-grained turbidites.
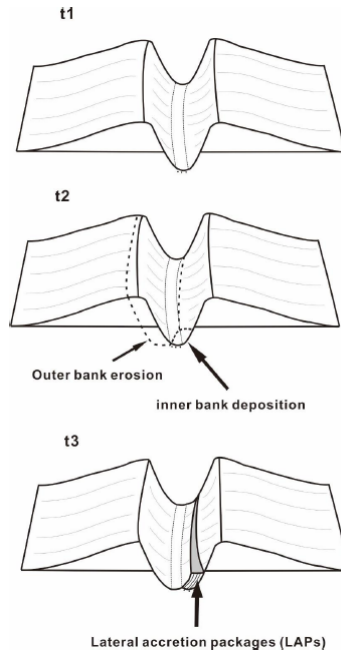
Figure 3.4: Continuous lateral migration within submarine channels (Qin, 2017). This process is similar to the formation of point-bars in fluvial channels and is characterized by the accumulation of Lateral Accretion Packages (LAPs).

3.4.2 Discrete migration

The discrete migration of submarine channels occurs in the form of cut-and-fill processes that involve the infilling of the channel before shifting its position, with flows eroding the channel banks and generating the remaining channel-fill deposits (Deptuck et al., 2007; Maier et al., 2012). Furthermore, during this process, turbidity currents can erode the inner or outer banks of previous channels, resulting in lateral migration with no clear patterns (Figure 3.5). In addition, Deptuck et al. (2007) suggest that the position of channels re-incision is strongly influenced by the thickness of channel-fill deposits. For example, thicker channel-fill deposits result in the reduced confinement of subsequent erosive flows and these flows are thus less likely to follow their previous pathways (Deptuck et al., 2007).
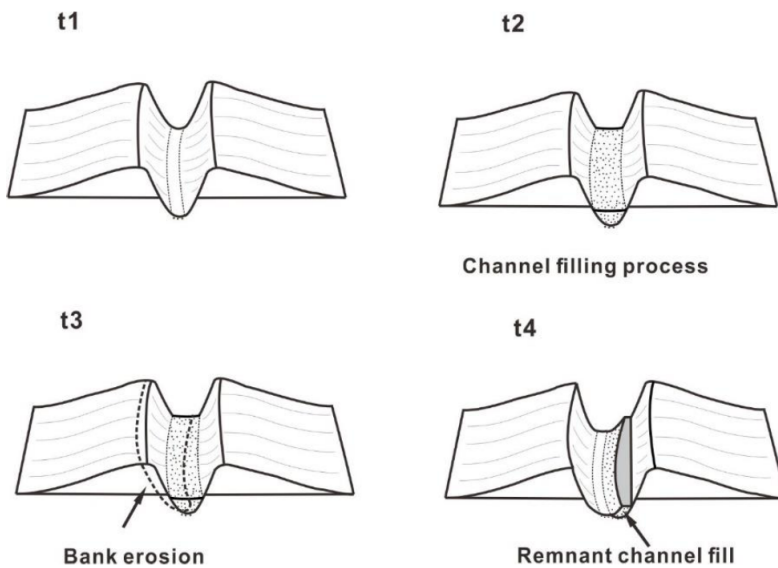
Figure 3.5: Discrete lateral migration within submarine channels (Qin, 2017). This figure illustrates a a cut-and-fill process involving the total infill of the channel before the channel shifts its position, with flows eroding the channel banks and generating remnant channel-fill deposits.

Chapter 4

Data and Methodology

4.1 Data

4.1.1 Seismic dataset

The primary dataset for this thesis consists of Waka 3D seismic reflection data which is located in the South-western part of the Canterbury Basin. In addition, the 2D seismic reflection data is used for the correlation of formation stratigraphic tops in the study area (Figure 4.1). The Waka 3D seismic reflection survey covers an area of 1150 km^2 and the data was acquired by 6×5100 m array of streamers. The survey has a bin spacing of 12.5 by 25 m and a 4 ms vertical sampling interval. The Waka 3D seismic reflection survey is the final stack, which was compiled by the New Zealand Petroleum and Minerals department (NZP&m). In addition, the data ranges from (1000-1550) in the inline direction and (835-6950) in the crossline direction.

4.1.2 Well Data

Two wellbores (Caravel-1 & Galleon-1) are used in the study area with Waka 3D seismic reflection survey (Figure 4.1). Caravel-1 was drilled inside the Waka 3D survey, by Anadarko New Zealand Company (ANZC), in 2014 and penetrated into the basement formation with a total depth of 2692 meter. Unfortunately, most of the log data for Caravel-1 is not acquire in the study interval (Figure 4.2). The log data acquired with different logs suite of (Sonic, density, resistivity, gamma-ray, and neutron porosity) whereas, only gamma-ray log data was acquired from 1130 meter to the basement but all other logs are just acquired in the reservoir section from (2127-2652) meters.
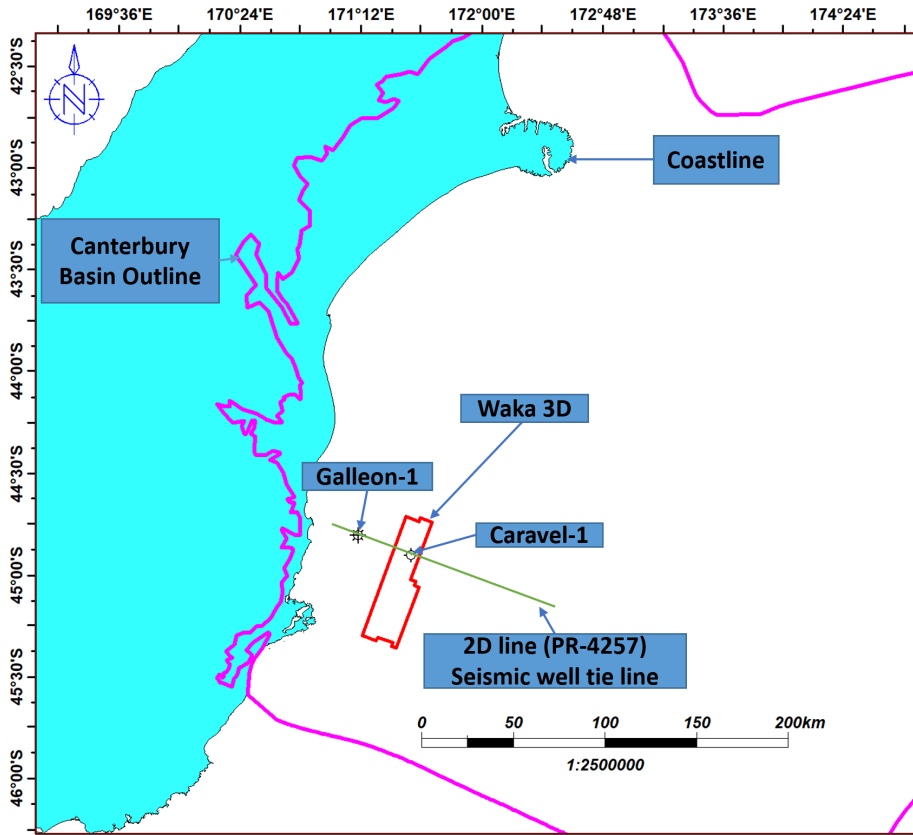
Figure 4.1: Basemap showing the location of the 3D seismic survey acquired over the Canterbury Basin, offshore New Zealand. The red Box denotes the boundary of the Waka-3D seismic reflection survey & green line is a 2D seismic line crossing both wells, whereas the Coastline and the Canterbury Basin Boundary also shown.

Galleon-1 is closest to the Waka 3D seismic reflection survey and located approximately 30km to the northwest direction drilled by Shell, BP, and Todd in 1985 (Figure 4.1). This well is penetrated to the total depth 3096 meters into the igneous basement. In addition, the log data acquired with different logs suite of (Sonic, density, resistivity, gamma-ray, and neutron porosity) whereas, the density log data acquired from 2710 meters to TD and sonic log data from 640 meters to TD, which is used for the construction of Synthetic Seismogram (Figure 4.2).
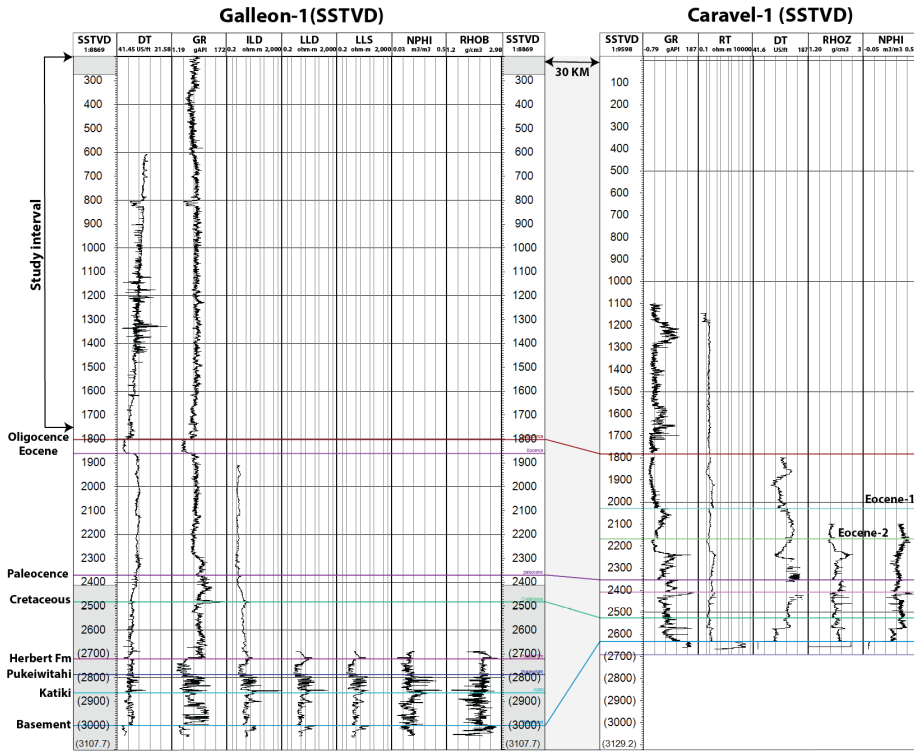
Figure 4.2: Stratigraphic cross section from Galleon-1 to Caravel-1 with log data and the study interval.

4.2 Data Quality and Key Components

4.2.1 Data Resolution

The vertical resolution of seismic data is defined as the vertical distance between two seismic reflections that can be resolved separately, and this separation relates to the distance between two interfaces (Hart, 2011). A value of ($\lambda/4$) is generally considered to define the vertical resolution of seismic data. Therefore, with higher frequency and lower the velocity of the wave, the vertical resolution will be better (Rafaelsen, 2006). However, as velocity increases and frequency decreases with depth, vertical resolution decreases (Figure 4.3).

The Lateral resolution of seismic data is associated with the Fresnel zone because the seismic energy travels as wavefronts, the region where the seismic energy is reflected constructively are known as the Fresnel zone (Rafaelsen, 2006). The width of an object equal to or greater than the diameter of the Fresnel Zone can be resolved in seismic data (Hart, 2011). The dominant frequency in the interested zone (1200-2200 ms) is 35 Hz, whereas the velocity of the Seabed is 1500 m/s and at Top Eocene level is 2500 m/s so the

average velocity in the zone of interest is about 2000 m/s. Hence, the vertical resolution is approximately 14 meter in the Waka 3D seismic reflection survey after incorporating the values of velocity and frequency. Furthermore, the dominant frequency of the 2D Seismic reflection data is approximately 35 Hz with an average velocity of 2,700 m/s hence, the vertical resolution of 2D seismic reflection data is approximately 20 meter.

Bed thickness > Tuning thickness   Bed thickness = Tuning thickness   Bed thickness < Tuning thickness

Limit of separability   No separability

$$\frac{\lambda}{4} = \frac{T}{2}$$

Amplitude boosted   Limit of visibility
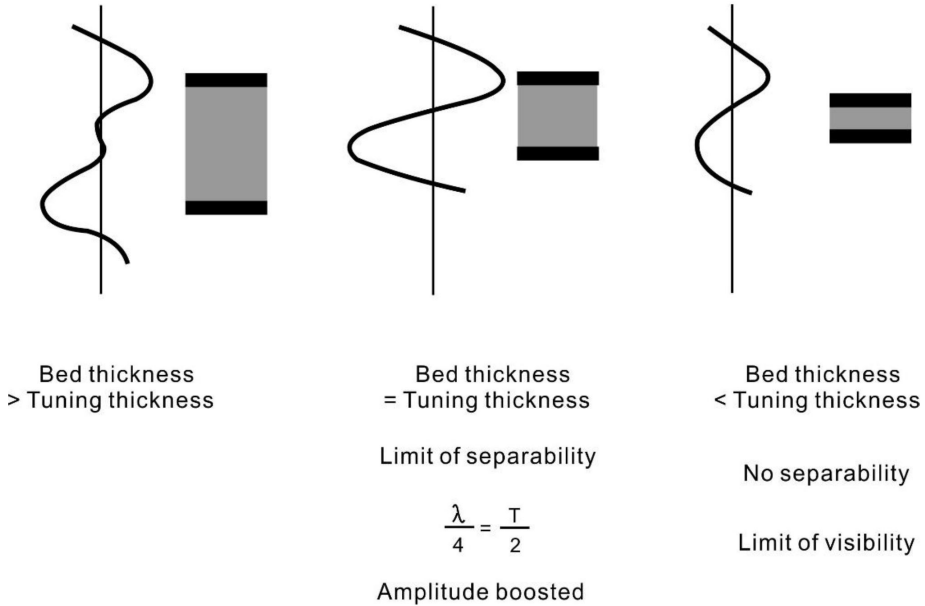
Figure 4.3: Resolution of the reflections from the top and bottom of a bed is dependent on the interaction of closely spaced wavelets (Brown, 2004).

4.2.2 Polarity

As per the recommendation of SEG committee on polarity published, by Thigpen et al. (1975) states that an upward geophone movement or increase in pressure on a hydrophone should be recorded as a negative number and displayed as a trough for SEG normal polarity standards (Figure 4.4). This definition is followed worldwide for seismic data recording and the implication is that a reflection will start with a trough for a positive reflection coefficient (positive or hard reflection). In addition, this positive reflection is a reference for the interpreter's to depict the polarity in seismic data (Simm et al., 2014).

The polarity conventions apply to symmetrical wavelet have been identified by Sheriff and Geldart (1995) with reference to a positive reflection. Furthermore, the negative standard polarity represented as a trough (i.e. negative number) whereas, the positive standard polarity represented as a peak (i.e. positive number) shown in (Figure 4.4).

Historically two types of polarity standard have been mostly followed. One of them is European or Australian standard (i.e. Reverse Polarity) and the other one is American Standard (i.e. Normal Polarity) as shown in (Figure 4.4). In addition, these conventions are sometimes informally referred to respectively as 'SEG' normal' and 'SEG reverse' polarity. In European or Australian polarity an increase in the impedance gives the negative amplitude, normally displayed as a white trough in wiggle trace and red intensity in color display, whereas in American polarity an increase in impedance gives positive amplitude, normally displayed as a black peak in wiggle display and blue intensity in color display (Simm et al., 2014).
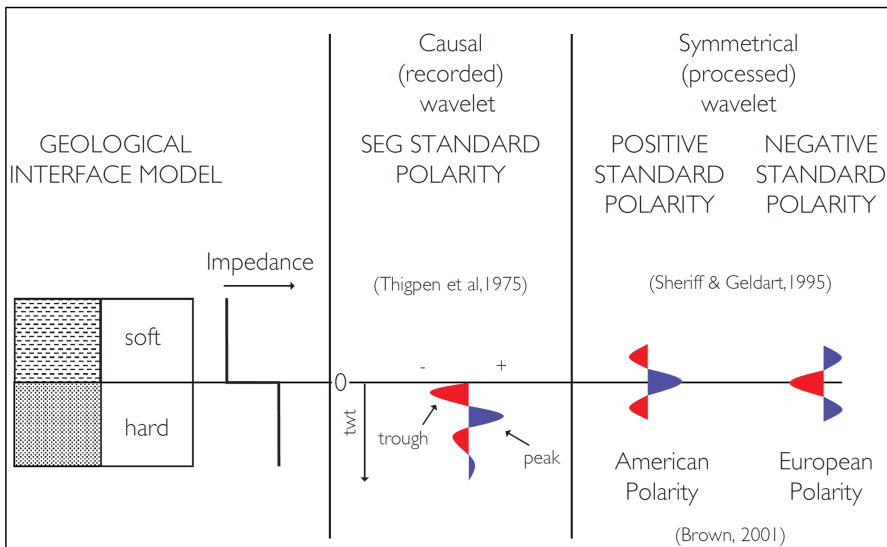
Figure 4.4: Polarity standards after (Simm et al., 2014).

The Waka 3D Seismic reflection survey is using the American polarity standards represented by peak wiggle trace which is surrounded by two side lobes (trough) and for this data the peak is represented by red color that shows the positive amplitude value whereas, the trough by blue color that shows the negative amplitude value (Figure 4.6). Furthermore, the first hard kick in Figure 4.6 is seabed which depicts an increase in the acoustic impedance and the difference in color represents the change in the amplitude. In addition, this change also links with the different properties in the sediments due to density, porosity and stiffness factors (Figure 4.6).

4.2.3   Phase

The phase of seismic data can be either Zero or Minimum. In standard seismic data processing, the Zero Phase data is preferred due to symmetrical wavelet, better correlation, better resolution, and amplitude are at the center of a wavelet (Figure 4.5). In seismic data the phase is considered as the time delay at the startup of the recording as it doesn't depend on amplitude so it is a good indicator for the continuity of seismic data even in the poor reflection zones, faults, pinch-outs and other seismic stratigraphic events (Brown, 2004).
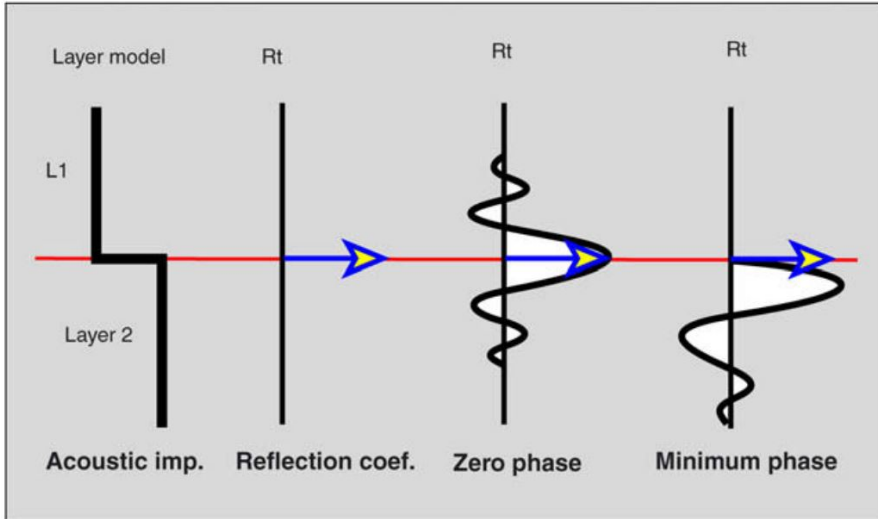
Figure 4.5: Typical minimum-phase and zero phase wavelets (Veeken, 2007).

The Zero phase data is mostly preferred as it required fewer efforts for processing and the data uncertainties are very less whereas, the minimum phase data display the false events as true events that lead to the wrong interpretation (Brown, 2004). The Waka 3D seismic reflection survey shows symmetrical wavelet and blue-red-blue density contrast sign of Mexican hat (Figure 4.6) illustrate the zero phase data.
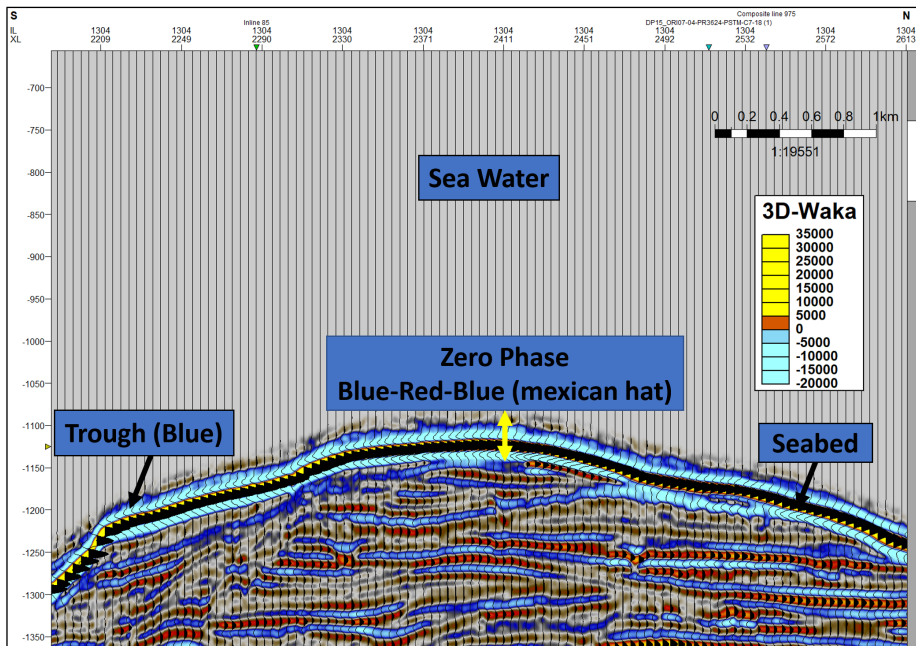
Figure 4.6: Polarity & Phase standards in Waka 3D seismic reflection survey.

4.2.4 Data Artifacts

Regardless of the advancement and accuracy of the acquisition, processing, interpretation equipment's and applied techniques, still there are natural limitation which can't be eliminated from the data and these constraints arises by complex geological features in the subsurface (Brown, 2005), anyhow these techniques helps to understand the complexity in more details to find out the real and true images of geological features. The volcanic intrusion in Waka 3D seismic reflection survey is quite prominent as shown in (Figure 4.7).

The amplitude variation in the data leads to false interpretation if phase, polarity and geological understanding of rocks are not understood. The bright amplitude in the data guides the interpreter for the hydrocarbon presence, but high amplitudes related with old age and at depth considered as discouraging for the presence of hydrocarbon (Brown, 2005). The amplitude variation in the Waka 3D seismic reflection survey is quite obvious (Figure 4.7) as it shows higher amplitude values which indicate fluid anomaly presence.
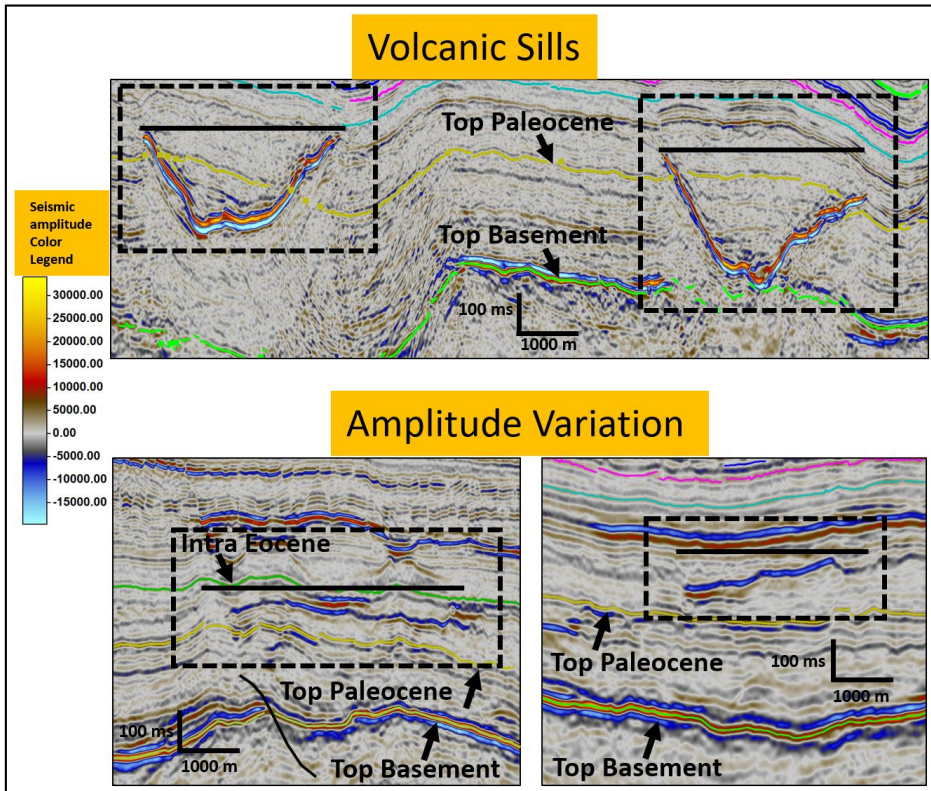
Figure 4.7: Seismic sections in Waka 3D seismic reflection survey shows the volcanic intrusion affected area & amplitude variation.

The lower velocity anomalies such as incised channels and canyons give rise to velocity push down. In addition, velocity pull-up and pull-down give rise to structures so sometimes they are mapped as ridges and valleys by the curvatures. Better migration techniques can help to reduce these effects and map the true features rather than the artifacts (Marfurt and Alves, 2015). The velocity push down are quite obvious in the Waka 3D seismic reflection survey (Figure 4.8) which effects the seismic data in most areas so it is challenging to differentiate between the real channel incisions and the depression created by velocity push down in the Waka 3D seismic reflection survey.
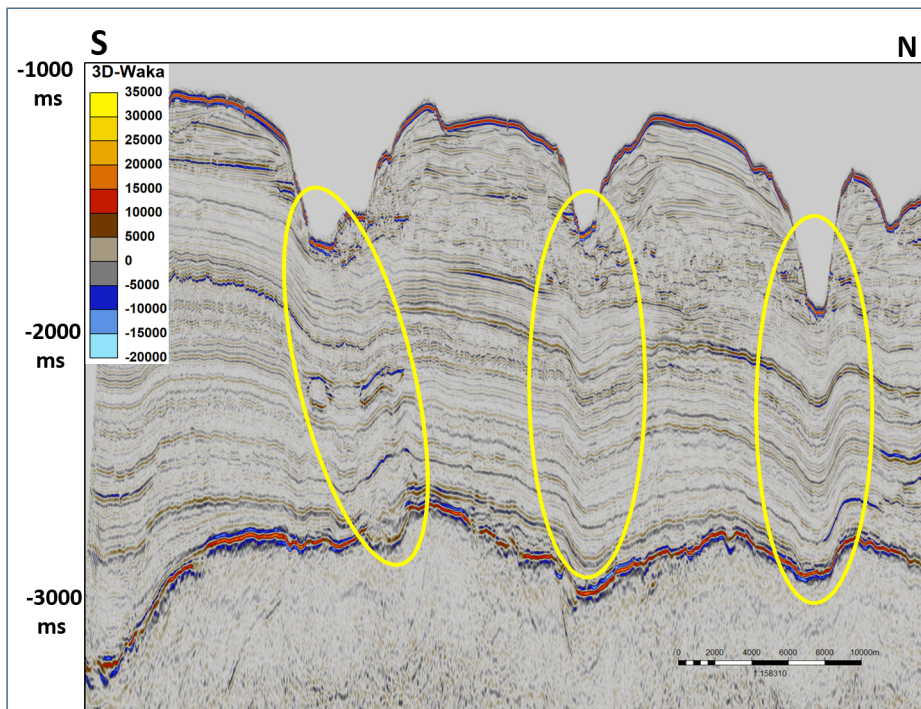
Figure 4.8: Velocity Push down effects in Waka 3D seismic reflection survey.

4.3 Methodology

The Seismic interpretation means the relationship between geology and geophysics. In this thesis, the focus of the interpretation is Quantitative Seismic Geomorphology, but to reach the final result it was important and essential to understanding all basic interpretation steps (Figure 4.9) which are as follow: 1) Well to seismic tie. 2) Seismic Faults interpretation. 3) Seismic Horizon interpretation.

The most important evaluation processes are focused on seismic geomorphological interpretation and facies analysis. To carry out this interpretation following methods are used: 1) Velocity Model and Seismic time to depth conversion. 2) Channel incision interpretation. 3) Seismic facies analysis. 4) Slicing Methods. 5) Seismic Attribute Analysis. 6) Morphometric Parameter Calculations.
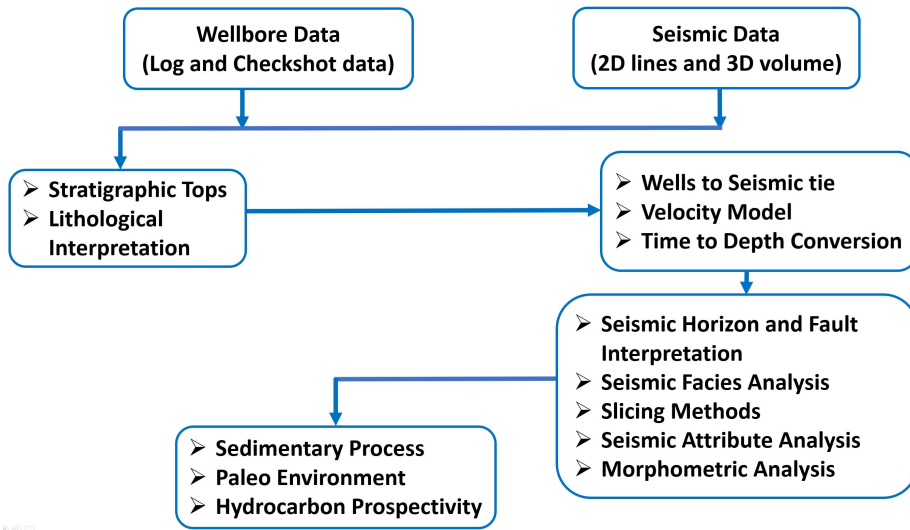
Figure 4.9: Thesis Workflow.

4.3.1 Well seismic tie

The Seismic, Well tie is the best way to tie seismic to the true ground information by comparison of the seismic image and well (hard) data, but the ground truth always needs fine-tuning before the comparison can be done (White and Simm, 2003).

The Seismic to well tie carried out by using the 2D Seismic line PR-4257 (Figure 4.1) which is passing through Galleon-01 and Caravel-01. The main reason for using Galleon-01 well instead of Caravel-01 is that it has more log information as compared to Caravel-01 where most of the logs are only acquired in the reservoir section. To find the best correlation for seismic to well tie Gardner Equation method (Gardner et al., 1974) is used and the seismic well-tie process was undertaken using check-shot, density and sonic log data from the wellbore in order to relate the seismic horizons to their appropriate depths (Figure 4.10).

The propose of sonic calibration is to integrate the travel times with sonic times for the depth domain in the wellbore. The time-depth pairs are recorded from the first break of VSP or Check shot survey. In addition, the sonic log is also recorded in the wellbore but it can be influenced by the cycle skipping effect and these factors can make some uncertainty in the sonic log reading, moreover the calibration performed by slightly increasing or decreasing the sonic slowness values over the section of the log between checkshot control points until the integrated sonic log travel times match those derived from the check-shot survey (Schlumberger, 2017).
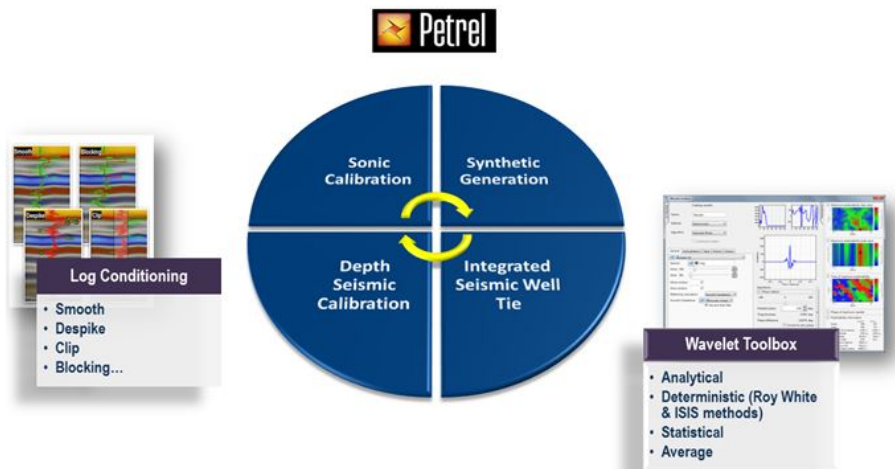
Figure 4.10: Petrel Well Seismic Tie Workflow (Schlumberger, 2017).

The recorded travel time of Galleon-01, wellbore and check-shot survey data are used to adjust the travel time of the integrated sonic log. The calibrated sonic log selected as the control time curve used to convert well logs from depth to time, both for display and for the generation of synthetics seismogram. The sonic log is affected by cycle skipping in the interval from 1150 meters to 1500 meters below KB (Figure 4.2).

The synthetic seismogram is a link between geological data and geophysical data that helps the interpreter for the following steps (Schlumberger, 2017):

- To establish an accurate time-depth relationship.

- Understand the phase characteristics of the seismic data.

- Tie between seismic horizons and geological markers.

- Seismic response of fluids and lithologies of the wellbore.

The basic process for the creation of synthetic seismogram required inputs as density and sonic logs which are multiplied together to get the impedance log or synthetic trace and this is converted to time. The resultant acoustic impedance is then used to compute the reflection coefficients at each interface between contrasting velocities which is used to build up the reflectivity series. The series is then convolved with the closed trace obtained from the seismic line from where the wellbore logs are acquired. The synthetic then correlates with both the seismic data and the wellbore log from which it was generated (Figure 4.11).
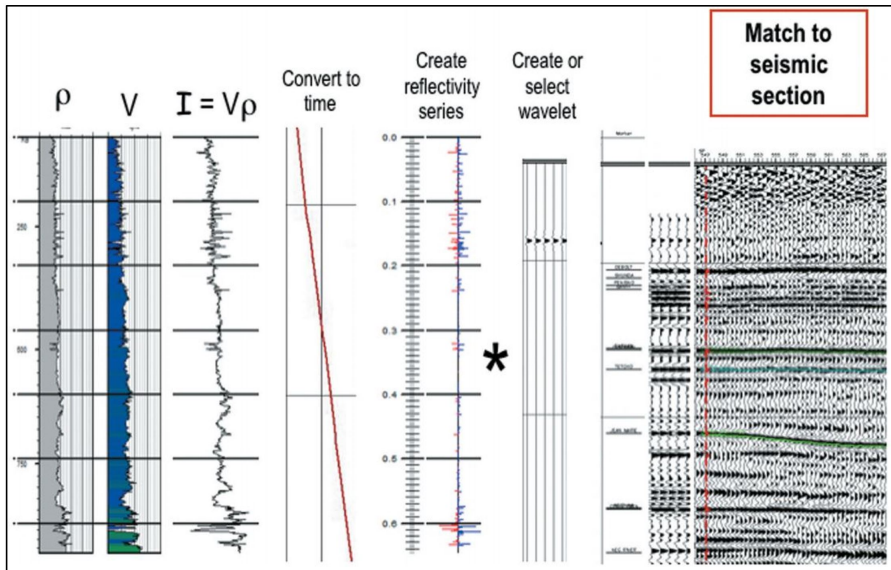
Figure 4.11: Cartoon describing the process of generating and correlating a synthetic (Anderson and Newrick, 2008).

4.3.2 Velocity Model and Seismic time to depth conversion

Velocity analysis is very important in finding the velocity trends and velocity functions that yield a proper velocity model for depth conversion. Furthermore, it is very important to find the best velocity model from the data analysis for correct depth conversion (Cannon, 2018). To remove structural errors inherent in time migration, it is necessary to convert time-migrated images into the depth domain either by migrating the original data with a prestack depth migration algorithm or by depth migrating post-stack data after time demigration (Kim et al., 1997). Each of these options requires a velocity model to convert the time domain data to depth domain data (Cameron et al., 2008).

The velocity model is build up by using the stratigraphic tops interpreted on the Waka 3D seismic reflection survey and the resultant time surfaces are multiplied with velocity values from (Mogg et al., 2008) to get the resultant velocity model. The primary input for the depth conversion is travel time and velocity data. Furthermore, the wellbore data are in depth domain so to make the exact correlation it is very important to convert the seismic domain from time to depth. In addition, the seismic depth domain data is better for accurate calculations of stratigraphic and morphometric parameters (Brown, 2004). Velocity model is the main input to convert the Waka 3D seismic reflection survey from time domain to depth domain. Depth conversion is calculated vertically, starting from the datum, progressing downwards and taking zone at a time (Figure 4.12). Each node looks upwards to find the time and depth in the layer above and from that, using the velocity model for the specified zone, the base of the zone is converted (Schlumberger, 2017).
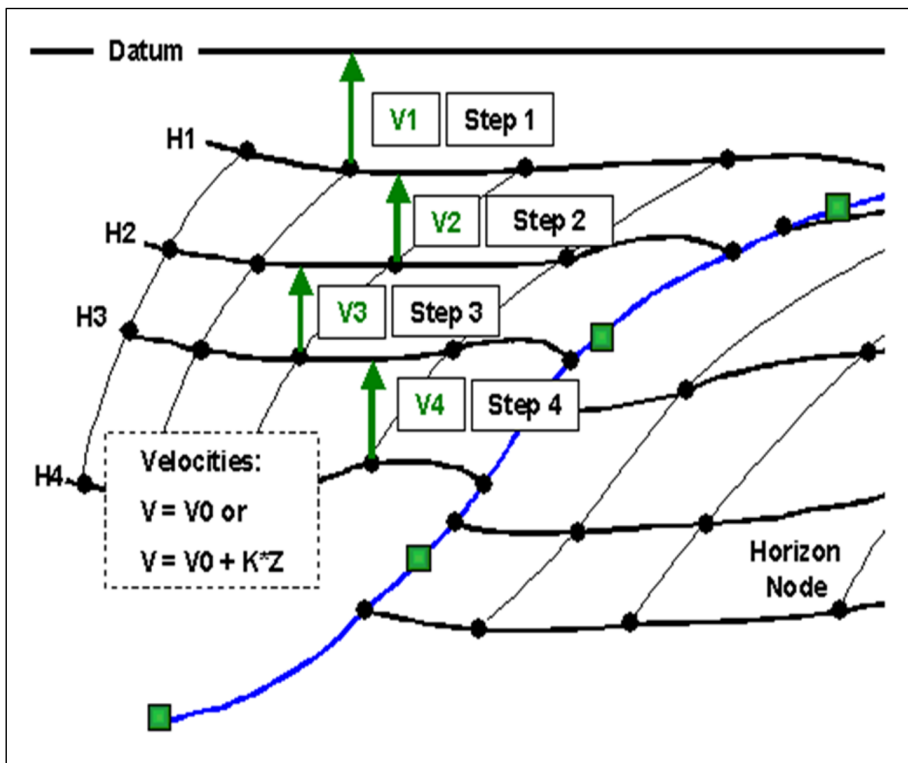
Figure 4.12: Basic principle of time to depth conversion (Schlumberger, 2017).

4.3.3   Seismic Horizon and Fault Interpretation

According to the Schlumberger Oilfield Glossary (1998), "horizon is an informal term used to denote a surface in or of rock or a distinctive layer of rock that might be represented by a reflection in seismic data". In seismic data, the horizon is having approximately the same amplitude values and are continuous in the lateral direction. The continuity and discontinuity depend on the geological object and noise in the seismic data (Verney et al., 2008). In addition, the discontinuous reflectors can be visually recognized by comparing their thickness, orientations, color and time relationship with other reflectors (Figure 4.13).

Seismic interpretation begins with mapping the structural elements of the various seismic reflectors or seismic events that are identified on processed seismic data. Geological settings and acquisitions details are important to know for interpreting seismic data. Furthermore, after the key seismic reflectors are identified then they are picked from trace to trace continuity throughout the seismic data. The horizon pick is further converted into structure map at top and base of the reservoir (Badley, 1985; Verney et al., 2008). In addition, some advanced techniques such as auto-picking, voxel tracking, interpolation, and surface slicing are also applied (Avseth et al., 2005).

The main challenge for horizon interpretation in Waka 3D seismic reflection survey is that from the basement up to top Paleocene, the data was influenced by volcanic intrusion, and it is hard to follow the seismic reflection continuity at some places. Moreover, the velocity push down was also an issue which leads to the miss interpretation of seismic horizon. The guided auto-tracking is used mostly in Waka 3D seismic reflection survey however, there are some parts where it didn't work due to data uncertainties causes by velocity push down and volcanic intrusions so, the manual interpretation was carried out in those regions.

According to the Schlumberger Oilfield Glossary (1998), "a fault is a break or planar surface in brittle rock across which there is observable displacement". The movement of the fault can be normal, reverse or strike-slip depends on the relative direction of the displacement between the rock or fault blocks on either side of the fault. In seismic data, the discontinuity makes the reflector gap which is dip fault (normal or reverse) mirror (Figure 4.13). In addition, faults also correspond to noisy zones (Verney et al., 2008). According to Badley (1985) there are some key steps to follow for fault analysis during seismic data interpretation.

- Fault correlation both vertically and laterally between the horizons.

- Geological consistency of interpreted horizons.

- Verify fault linkage patterns and kinematic coherence between members of a fault array.

- To assess the viability of interpreted fault geometry.

- Quantify fault displacement and growth histories.

Furthermore, the Polygonal fault system is mainly found in fine grain sediments controlled by vertical layers and identified by polygonal planform geometry. In addition, they are represented by small throw, high fault density, small extensions, and various strikes. Moreover, their genetic mechanism usually recognized as non-tectonic which include dewatering contraction, gravity loading, density inversion and dissolution-induced shear failure (Xiujian et al., 2013). These faults occur because of the development of polygonal faults discontinues temporarily as a result of a change in regional sedimentation leading to inactive polygonal faults and the faults are confined to stratigraphic horizons with observed distinct spacing among faults (Cartwright, 1994). The formation of these features is linked to differences in lithologies and volumetric contraction of the fine-grained sediments leading to pore fluid expulsion (Lonergan et al., 1998).

Figure 4.13: Horizon and Faults ontology (Verney et al., 2008).

4.3.4 Seismic facies analysis

Seismic facies analysis means the interpretation of the environment and lithologies from seismic reflection data (Mitchum Jr et al., 1977). It comprises the delineation and interpretation of reflection parameters, as well as the external and three-dimensional associations of groups of reflection patterns; produced by reflection geometry, continuity, amplitude, frequency, and interval velocity.

Seismic facies units are three-dimensionally traced and they consist of areas where specific reflection characteristics are detected (Sangree and Widmier, 1977). The following elements are important to consider for seismic facies analysis to interpret the depositional environments and lithofacies distribution.

- Reflection termination Patterns
- Internal reflection configuration
- Amplitude
- Frequency
- Reflection Continuity
- External Geometry

The reflection terminations are named according to their angular relationship with underlying and overlying bounding surfaces (Vail, 1987). The following termination patterns are identified on the seismic data. 1) Erosional truncation is the termination of strata against an overlying erosional surface. 2) Apparent truncation is the termination of relatively low angle seismic reflections beneath a dipping seismic surface. 3) Onlap are recognized on the seismic data by the termination of low angle reflections against a steeper seismic surface. 4) Downlap are initially inclined stratum terminates downdip against an initially horizontal or inclined surface. 5) Toplap is the termination of inclined reflections against an overlying lower angle surface to represent the proximal depositional limit. 6) Offlap is a conformable sequence of inclined strata, deposited during a marine regression, in which each stratum is succeeded laterally by progressively younger units (Figure 4.14).

The major reflection configurations are recognized with the help of seismic data and then each of them is interpreted in terms of depositional environment and lithofacies distribution (Mitchum Jr et al., 1977). The following geometries can be distinguished: 1) Parallel or sub-parallel. 2) Wavy. 3) Divergent. 4) Clinoforms. 5) Shingled (low-angle foresetted with low foreset height). 6) Hummocky (some degree of the internal organization). 7) Chaotic. 8) Reflection-free or transparent (Figure 4.15).
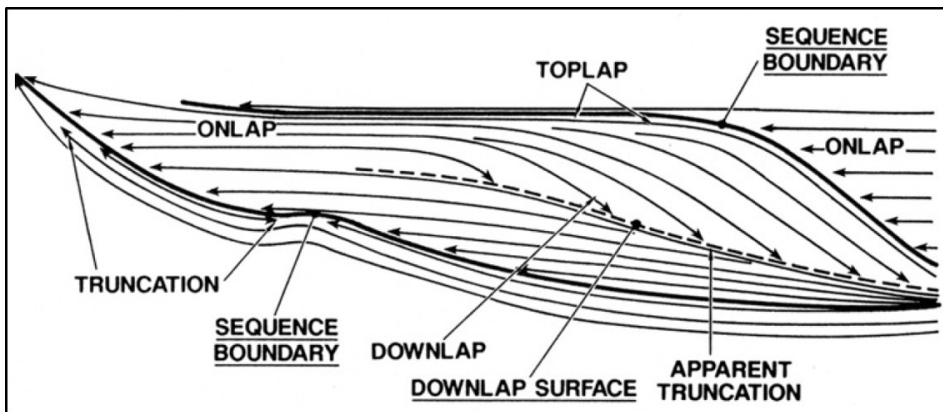
Figure 4.14: Diagram showing reflection termination patterns and types of discontinuities (Vail, 1987).
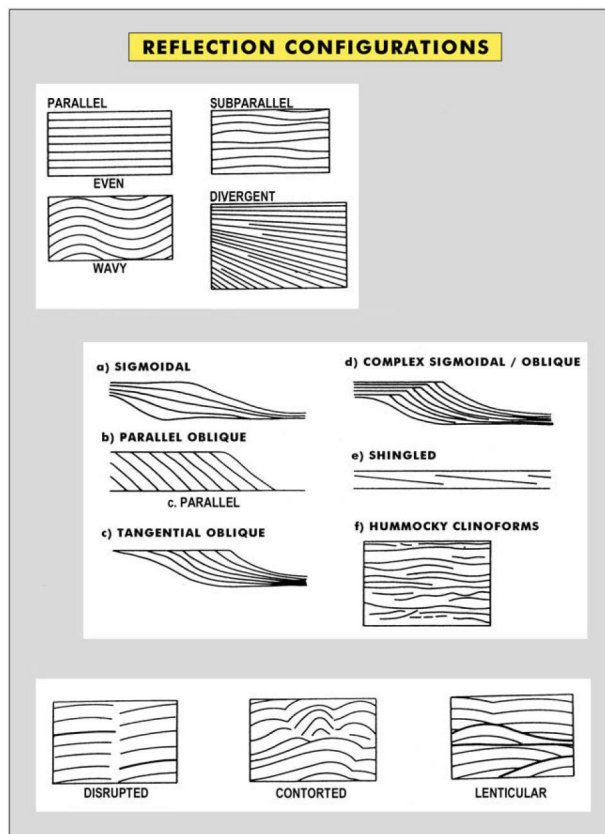
Figure 4.15: Reflection geometries and their interpretation (Mitchum Jr et al., 1977).

Reflection amplitude is a function of the energy of seismic waves and is directly proportional to reflection coefficient. Amplitude is a measure of the strength of the reflections since the proportion of the energy reflected at the boundary between two beds is a function of the difference in the acoustic impedance's (Badley, 1985). The amplitude can be low, High, Medium to Moderate, Transparent, Incoherent and this variation in the amplitude used to identify the bed spacing, Bed thickness and Fluid contents for geological interpretation (Figure 4.16).

Frequency or spacing describes the number of reflectors per unit time. It is a good sedimentary facies discriminator. As the vertical changes in reflector spacing can be used as a guide for locating boundaries between depositional sequences. The descriptive terminologies are low or high frequency (Badley, 1985) and this variation helps to find the geological interpretation for the bed thickness and fluid content (Figure 4.16).

The continuity of reflectors is a function of how continuous the sediment beds are and also depends on the degree of contrast across the interface, its extents, and nature. The continuity of seismic reflectors is usually associated with the lateral extension of uniform strata (Badley, 1985). The descriptive terminologies are continuous, less continuous, high continuous, discontinuous, faulted and continuous. This variation helps to find the lateral continuity of strata and depositional processes (Figure 4.16).
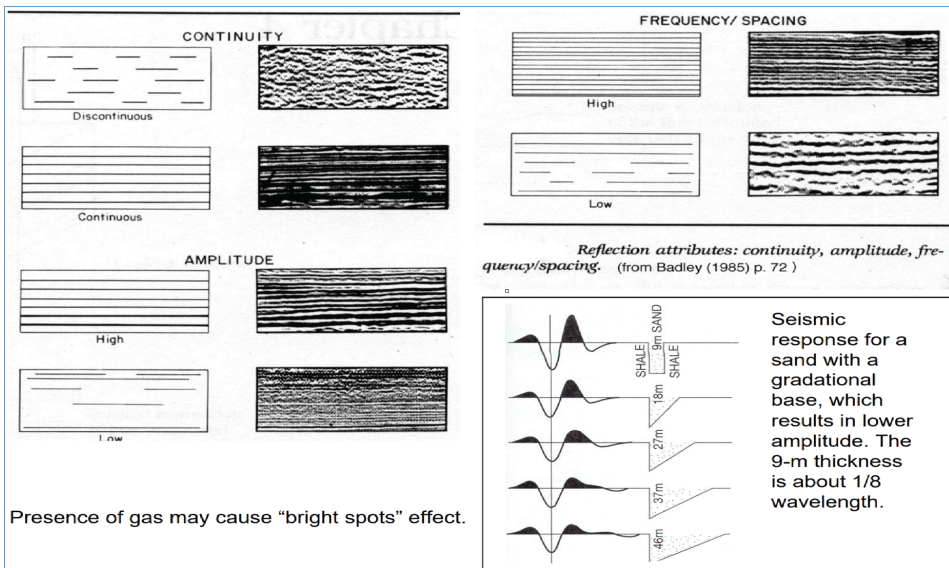
Figure 4.16: Reflection attribute continuity, amplitude, frequency spacing (Badley, 1985).

After the delineation of Seismic facies on the seismic sections, the external geometry help to figure out the Gross depositional environment, Sediment source, Geologic setting in the area (Vail, 1987). These external geometries are sheet-drape (low energy), slope front fill (low energy), Onlap fill (usually low energy), fan complex (High energy), Contourite

(Variable energy), mounded Onlap fill (High energy), and chaotic fill with variable energy (Figure 4.17).
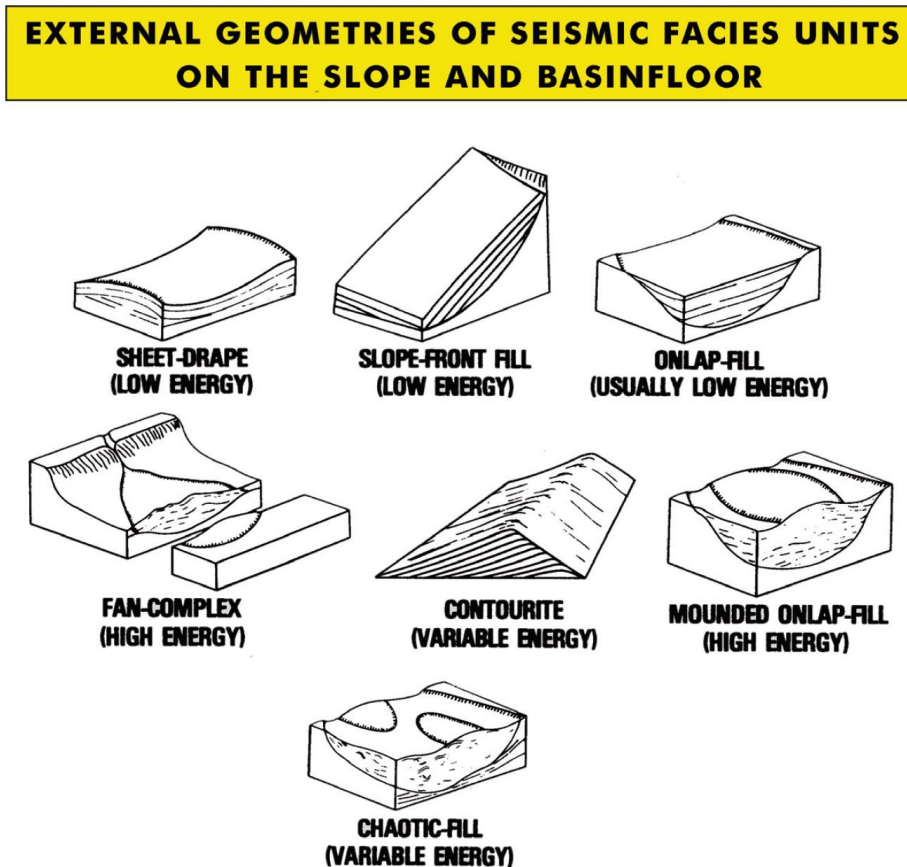
Figure 4.17: Various external geometries of seismic facies units in a slope and basinal areas (Vail, 1987).

4.3.5 Slicing Methods

3D seismic technology brought a major change to seismic interpretation, one of them is the ability to correlate the interpretation of geology by using the horizontal seismic resolution and the other one is improving the interpretation of petroleum systems and reservoirs, especially thin beds near or below seismic resolution (Zeng, 2010).

There are three methods commonly used for the slicing. The First one is the Time slice which is the earliest form of horizontal seismic display and is good for sheet-like and flat-laying formations as explained by Zeng et al. (2011) and shown in (Figure 4.18). Furthermore, the Time slices are extracted from a 3D data volume (Zeng, 2010) at a constant

image-time coordinate. The Second one is the Horizon Slicing and it can handle better sheet-like structure but not flat-lying strata (Zeng et al., 2011). In addition, the horizon slice is constructed by extracting a seismic attribute parallel to a picked time-varying horizon as explained by Zeng (2010) and shown in (Figure 4.18).
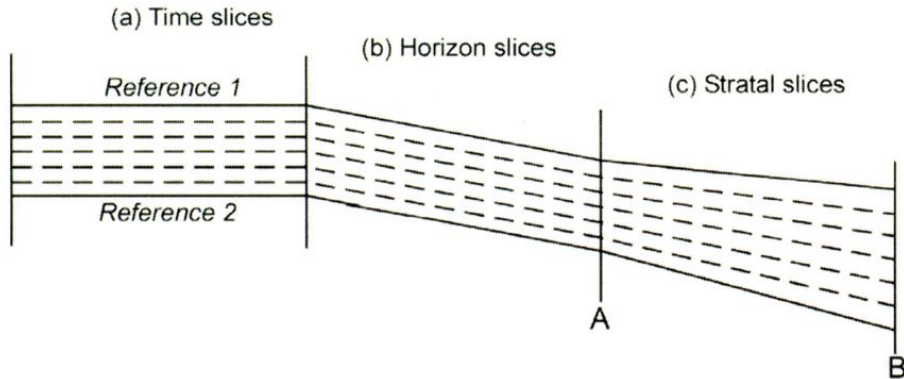
Figure 4.18: Distinctions among time slices, horizon slices, and stratal slices (Zeng, 2006).

The third one is the Stratal slicing method which is more challenging as compared to another methods because sometime the seismic event does not necessarily follow an impedance boundary defined by a geological time surface (Zeng et al., 1998). Stratal slicing required to pick up the geological time surface so any attribute drive from such a surface could represent genetic depositional unit (Figure 4.18) and it is important for this method to have satisfactory geological and geophysical conditions. First, a good quality geological time framework (time-parallel reference events) should be in place before slicing; second, depositional system in the basin fill should be deposited along with a linear lateral thickness change; third, there should be no significant angular unconformity; fourth, reflection energy of the target should be strong enough to be detected as a seismic event and finally, the displayed attribute should share a simple relationship with the reservoir property of interest (Zeng, 2010).

4.3.6 Seismic Attribute Analysis

Seismic attributes are the fundamentals of seismic data which can be extracted from seismic data by computation, measurement, and other methods (Subrahmanyam and Rao, 2008). The attributes are divided into geometrical and physical classes where dip, azimuth, and continuity include in the geometrical attribute which is used to enhance the visibility of the geometrical characteristics of seismic data. On the other hand, physical attributes are related to physical parameters of the subsurface and they are relevant to lithology. The Physical attribute includes amplitude, phase, attenuation, and frequency. Furthermore, the classification in Figure 4.19 can be divided into prestack and poststack attributes (Chopra and Marfurt, 2005).

In general, the time derived attributes provide structural information, amplitude derived provide stratigraphic and reservoir, frequency derived additional stratigraphic and reservoir information and attenuation is related to the permeability information. However, poststack attribute can be extracted along one horizon or summed over a window and if the window is a constant float time interval then the resultant attribute will be thick time slice, sometimes call the statistical slice, On the other hand the variation of the attribute within the window may be measured to assess a distribution. The prestack attribute measures the variation as a function of angle of incidence (source to receiver offset) and the main example of these are AVO (Brown, 2004).
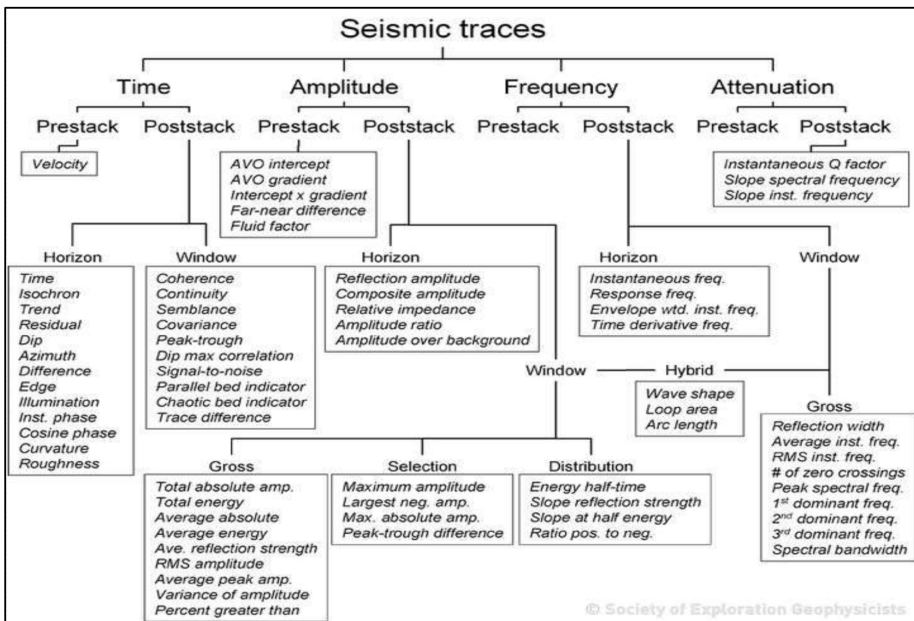
Figure 4.19: Seismic attributes derived from or related to the basic seismic information of time, amplitude, frequency and attenuation. Window can be a constant time interval, constant interval hung from one horizon or interval between two horizons (Brown, 2004).

According to the discrete frequency characteristics of the tuning volume of a thin layer, the frequency decomposition technique identifies distribution characteristics of thin layers by analyzing the frequency characteristics of complex formations and regional phase characteristics. It is a new method of seismic interpretation with powerful imaging and simulation techniques for delineating discontinuous geological bodies and stratigraphic thicknesses (Li and Zhao, 2014). Spectral decomposition was used to image subtle frequency variations at the base of each terrace to identify depositional elements whose scale is below the average seismic resolution of the full-stack data. Since the peak frequency response for a specific seismic interval varies with its temporal thickness (with higher frequencies imaging thinner geological features), so visually blending a number of discrete frequency bands can reveal subtle changes in thickness and therefore, sedimentological

features can be identified that are otherwise difficult to detect on conventional amplitude maps (Hansen et al., 2017).). Furthermore, the Mixer of discrete frequency is an intuitive and interactive visualization tool that enables to visually compare and evaluate multiple seismic cubes simultaneously and synchronously, using RGB/CMY blend and mask workflows (Schlumberger, 2017). The Mixer tool is used to generate the spectral decomposition attribute by mixing the extracted frequency volume.

The RMS attribute is good in identifying the strong amplitude anomaly in the lateral environment and for the recognition of stratigraphic sequences. RMS attribute doesn't work well to detect the reflections inside the body of the channel (Lin et al., 2018). Variance attribute is used to find the similarity of traces and wave shapes within the chosen vertical window and this works well for the detection of faults, unconformities, fractures and channel infills (Pigott et al., 2013; Schlumberger, 2017). In addition, the variance attribute works well to detect the discontinuities that occur due to the structures and stratigraphic features, lithologies and the presence of oil and gas (Marfurt et al., 1998). But when variance and RMS attribute are combined together they work well for the detection of edges of the channel system.

4.3.7 Morphometric Parameter Calculations

The quantitative analyses of the channel system followed the methods of Deptuck et al. (2007); Qin et al. (2016); Gamboa and Alves (2015) and Hansen et al. (2017) represented in the (Figure 4.20). The incision interpretation of channels is completed on the entire Waka 3D seismic reflection survey, that involved a combination of manual and auto tracking procedures and later these incision interpretations are converted into the incision (channel) surfaces. The cross-sections are drawn perpendicular to these incision surfaces to calculate the morphometric parameters measured at an interval of 150-m average (the zero points is located in the proximal area).

The morphological analyses as shown in Figure 4.20 is carried on the interpreted incision (channel) surfaces in the Waka 3D seismic reflection survey that includes the channel height (i.e. distance between top of erosional banks and channel thalweg), width of channel floor (i.e. the length of horizontal to sub-horizontal part of the channel), width of channel (i.e. the distance between internal levee crests), aspect ratio (width/height) and cross-sectional area (CSA), sinuosity (i.e. the length between reference point and along channel axis) and channel gradient is calculated based on thalweg depth changes along the channel distance (Deptuck et al., 2007; Qin et al., 2016; Gamboa and Alves, 2015).

The erosional surfaces of the channel consist of bases, levees, and walls of the incisions whereas, the base is usually the low area on the erosional surface of a channel and the lowest point of the channel is called the thalweg (Figure 4.20) . In addition, the wall of a channel is a steep-sided area on an erosional surface and the levee is an area that converge away from the channel thalweg also the terrace is defined as a topographically flat area between a thalweg and wall (Harishidayat et al., 2018)
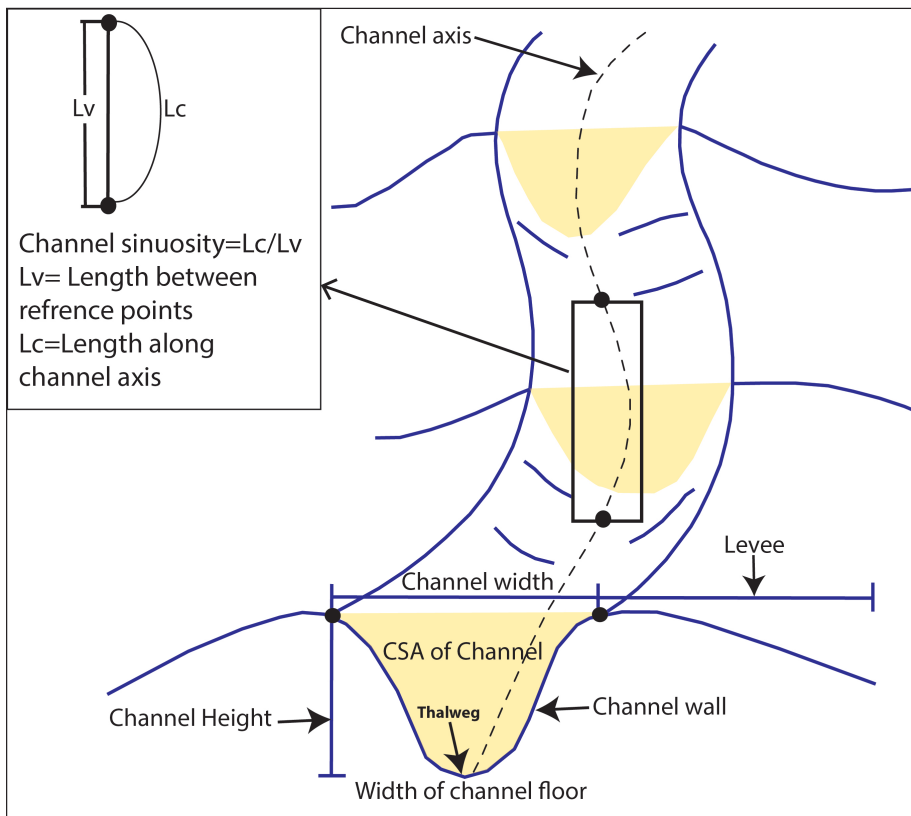
Figure 4.20: Schematic representation of morphological analyses commonly used in the interpretation channels modified after Qin (2017). Parameters analyzed include the channel-floor width, channel width, height, cross-sectional area (CSA), and channel sinuosity.

Furthermore, 'R' is the correlation for coefficient that measures the direction and strength of a linear relationship between two variables on the cross-plots, where R^2 is a coefficient of determination that measure the proportion of the variance (fluctuation) of one variable that is predictable from the other variable on the cross-plots (James et al., 2013). The channel sinuosity is measured as a ratio between the length along the channel axis and between the reference points as explained by Wynn et al. (2007) and shown in (Figure 4.20). In addition, the detailed sinuosity classification by Reimchen et al. (2016) has been used in the study area. The low sinuosity system is defined between the values 1.05 and 1.2, whereas, for the straight channel systems the values are between 1.0 to 1.05, and for the high sinuosity system the values are greater than 1.2. Furthermore, the aspect rations between widths and heights of the channel systems are also described and by definition the proximal, medial and distal areas of the channels are based on the gradient of the channel systems.

Chapter 5

Results

5.1 Synthetic Seismogram

The synthetic seismogram in Figure 5.1 shows the correlation between seismic data and the synthetic trace generated using the Galleon-1 wellbore data information. The sonic log shows higher values from (2830 to 2900 meter) at Cretaceous level due to the presence of coal seams (Figure 2.3). In addition, the noisy data & tool problem can also effects the sonic log readings in these zones (Figure 5.1). The study interval for this work is shown in Figure 5.1 which starts from Top Oligocene up-to-the Seabed. Furthermore, the density log (RHOB) shows too many deflections as shown in blue color due to the bad hole conditions possibly washouts in most part of the section that disturb the density log reading whereas, the sonic log (DT) shown in black color works well even in the bad hole condition according to sonic log principal. Overall, the seismic section shows better data quality and resolution in most parts which are used for the synthetic correlation (Figure 5.1).
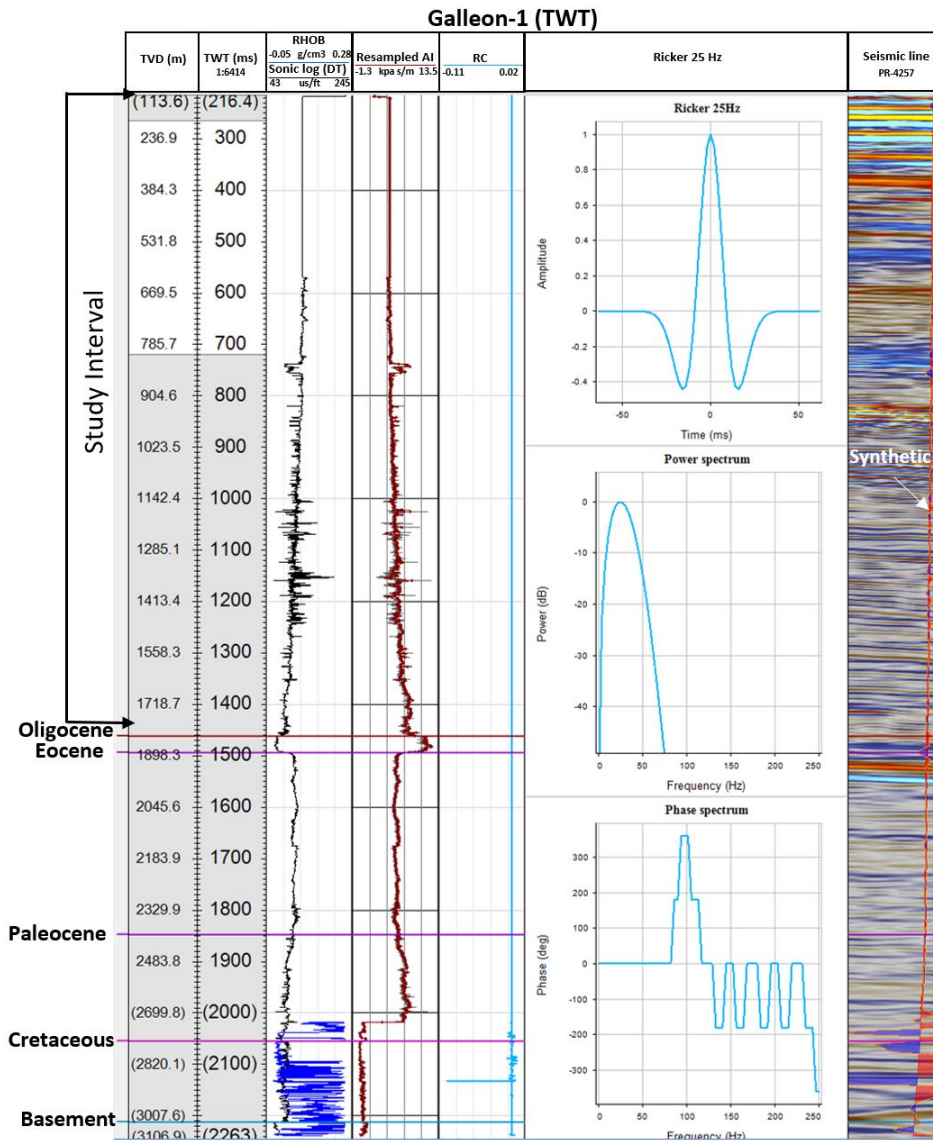
Figure 5.1: Synthetic Seismogram with Galleon-1 Wellbore and 2D seismic line PR-4257. See Figure 4.1 for the location of Galleon-1 wellbore and PR-4257 seismic line.

5.2 Velocity Model

The resultant velocity model in Figure 5.2 shows the average velocity behavior in the Waka 3D seismic reflection survey. The velocity variation is very evident in the Waka 3D

seismic reflection survey due to the presence of volcanic intrusions. The seabed velocity is 1500 m/s whereas the basement velocity is around 2900 m/s. The velocity variation is very prominent between (2000 to 2400 m/s) where the volcanic intrusion is mostly present. In addition, the study interval is highlighted in the Figure 5.2 which depict the velocity behavior is smooth and the volcanic intrusion effect is not too much in the study interval Moreover, the velocity push down effects also create velocity variation which is also present in Waka 3D seismic reflection survey. The time domain Waka 3D seismic survey is converted into depth domain using the velocity cube information from Figure 5.2 which helps to convert the time domain Waka 3D seismic survey into depth domain which is further used for the morphometric parameter calculations.
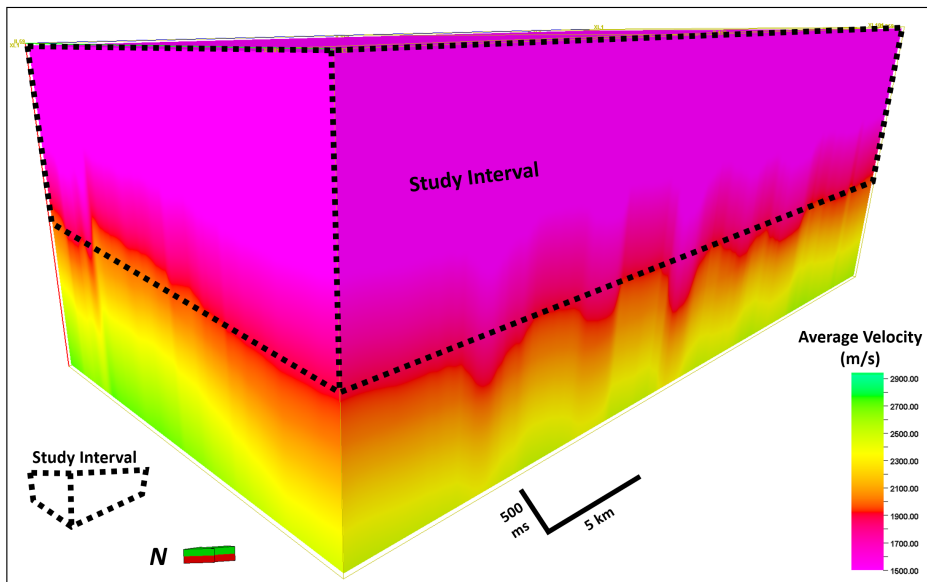
Figure 5.2: Velocity model of Waka 3D seismic reflection survey.

5.3 Seismic Horizon and Fault interpretation

Six main horizons (Basement, Top Cretaceous, Top Paleocene, Top Eocene, Top Oligocene & Seabed) are interpreted in this Waka 3D seismic reflecion survey (Figure 5.3). The Horizon interpretation is based on seismic to well tie information obtained from Galleon-1 wellbore and 2D seismic line (PR-4257). In addition, the 2D Seismic line (PR-4257) also crosses the Waka 3D seismic reflection survey and Caravel-1 wellbore (Figure 5.3).
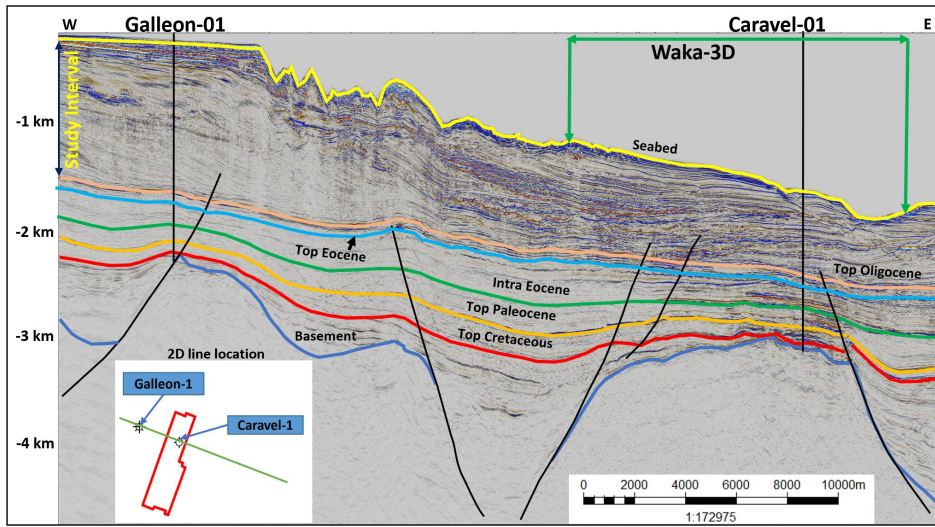
Figure 5.3: 2D seismic tie line through Galleon-1 and Caravel-1 locations.

Five key horizons have been mapped (Figure 5.4) in Waka 3D Seismic reflection survey (i.e. Seabed, top Eocene, top Paleocene, top Cretaceous & Basement) and the horizon tops information is obtained from the 2D seismic line which includes the seismic well tie with Caravel-1 and Galleon-1 (Figure 5.3). The correlation of stratigraphic with the seismic is obtained from synthetic seismogram in (Figure 5.1). The resultant surfaces show the variation within the Waka 3D seismic reflectin survey where the seabed surface clearly shows the presence of channels incisions, but for the deeper horizons from top Eocene to basement, variations are mostly due to velocity push down and the presence of volcanic intrusion in some parts (Figure 5.4).

The fault framework is build using the Waka 3D seismic reflection survey and display along the variance attribute to show the faults behavior in the Waka 3D seismic survey. The fault system in this Waka 3D seismic reflection survey is dominated by normal faulting and major faults are trending in NE-SW direction (Figure 5.5).
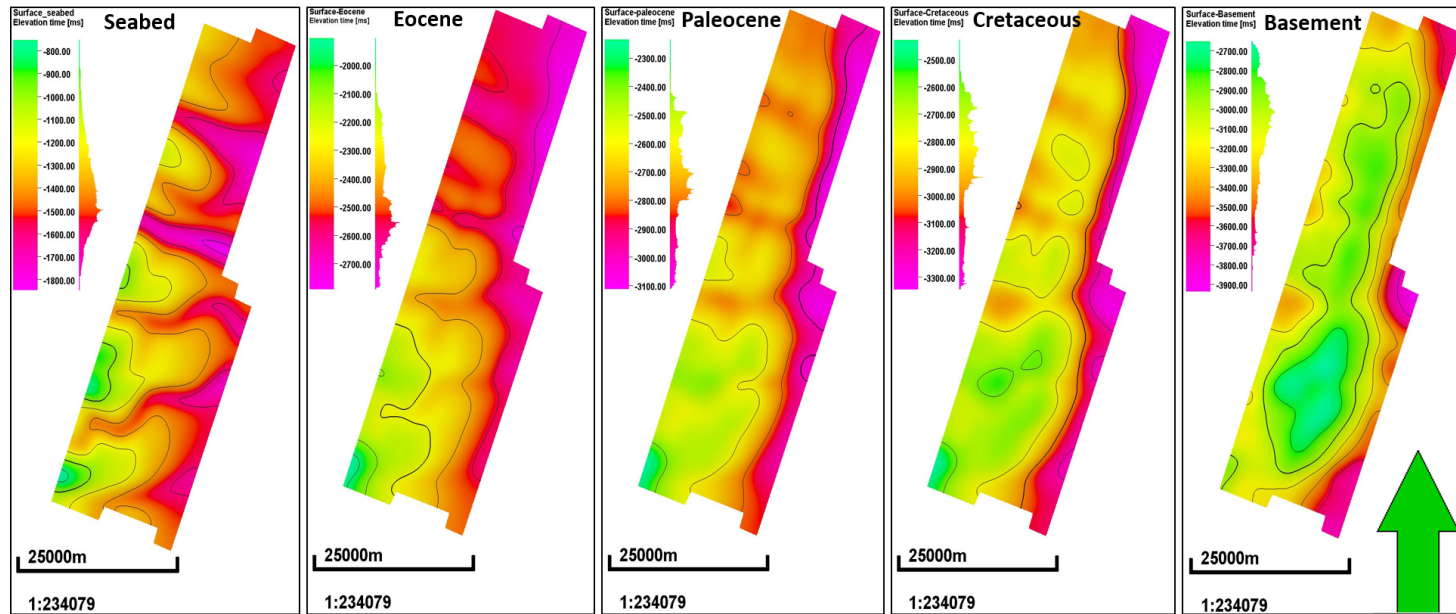
Figure 5.4: Time contour maps from the seabed to basement.
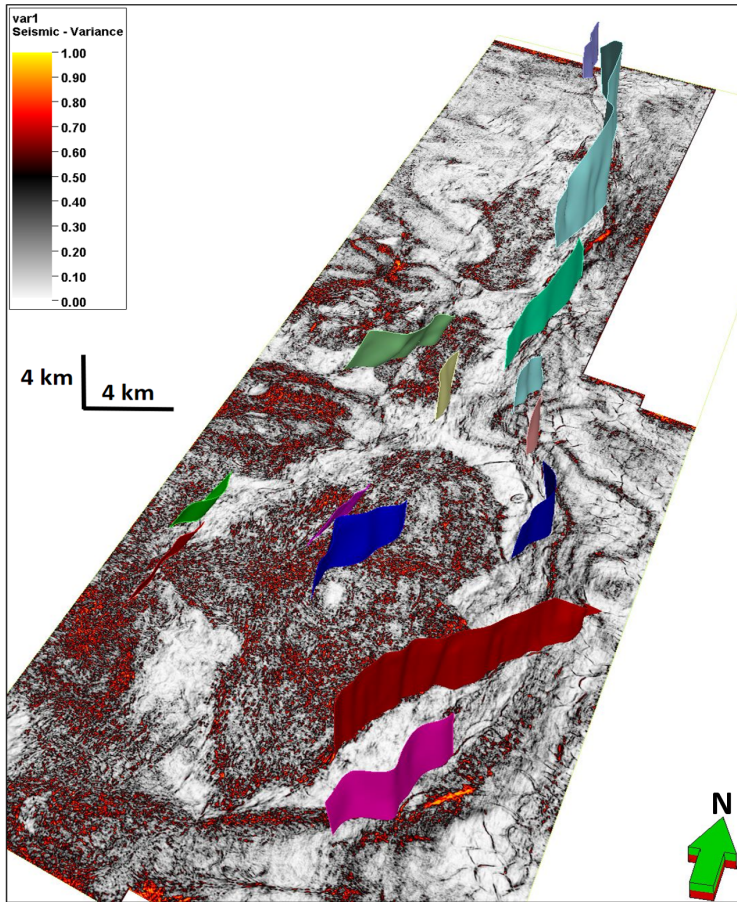
Figure 5.5: Fault framework at Top Eocene level with time slice information from variance attribute.

5.4 Slicing Result

Slicing results for three different techniques are shown in (Figure 5.6). Firstly, time slice technique is implemented to find out the channel orientations and migration in the available Waka 3D seismic reflection data as the time slice is a quick and convenient way to evaluate changes in amplitudes values of 3D seismic reflection survey, however, channel system is not too prominent (Figure 5.6a). Furthermore, the horizon slice technique depicts the presence of channel system which is extracted along the interpreted horizon (Figure 5.6b) in Waka 3D seismic reflection survey and the stratal slice technique also shows the presence of a channel system which is extracted between two interpreted horizons (Figure 5.6c) in Waka 3D seismic reflection survey. Overall the slicing methods result in Waka 3D seismic reflection survey shows the presence of a channel system.
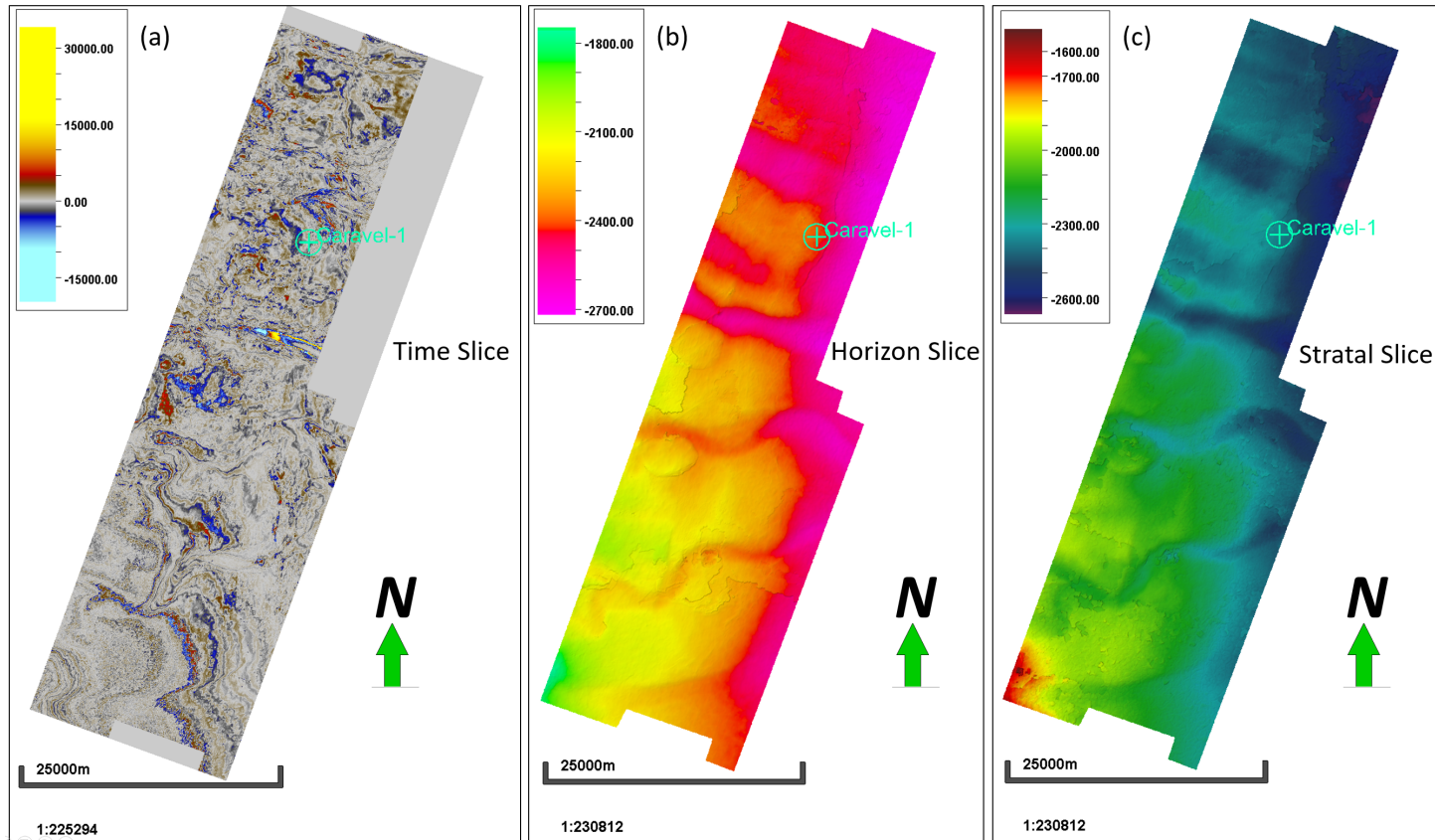
Figure 5.6: Slicing methods result.

5.5 Attribute analysis

After the channel feature is identified from the horizon and stratal slicing, the seismic attribute analysis is performed to be able to identify the geometry and architectural elements of the channel feature. In addition, the Spectral decomposition attribute is generated to evaluate the channels in the Waka 3D seismic reflection survey. Furthermore, this survey is decomposed into three amplitude-response volumes, each with a different average frequency: 10 Hz, 20 Hz and 30 Hz extracted from the study interval (Figure 5.3) by using frequency spectrum analysis.
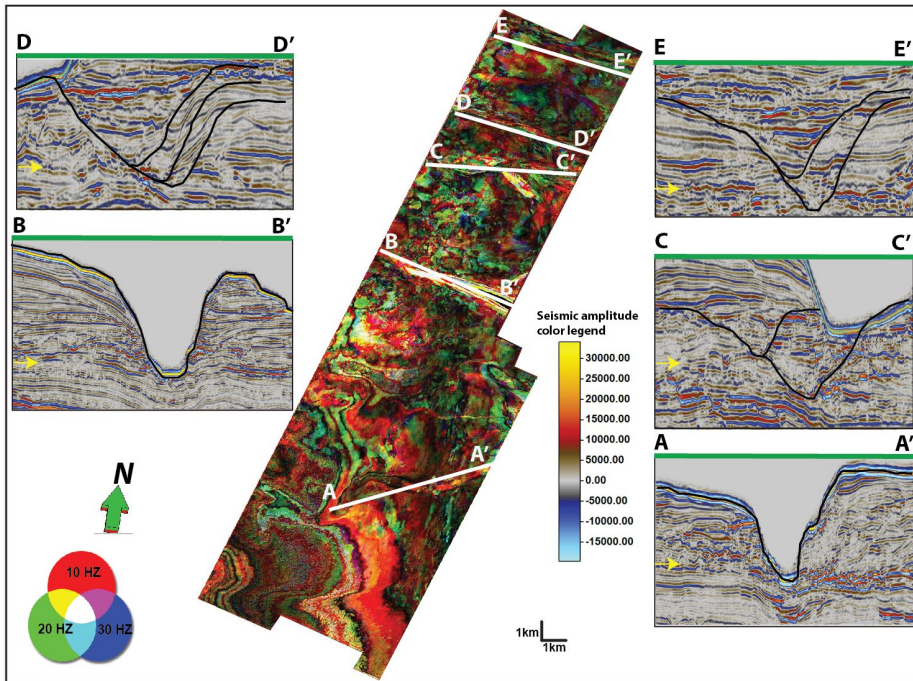
Figure 5.7: Spectral decomposition seismic attribute result of the time slice. Note that the yellow arrow on the seismic section profile is the location of the time slice.

5.6 Morphological analysis of sediments conduits

Eighteen (18) channels are identified within the study area in the Canterbury basin having V and U shaped morphologies with stacked and single channels system (Figure 5.8). Four representative channels type are selected to investigate in detail, the morphometric elements and it's facies in the Waka 3D seismic reflection survey (Figure 5.9). These channels are mainly oriented in NE to SW direction reflecting the overall channels trends in the Canterbury basin (Figure 5.8).

The four elements of channel surface architectures are found in the study area, these are: (thalwegs, terraces, walls, and levees) that include V and U shaped bases (Figure 5.9). Furthermore, the V-shape channels are the most common in the study area while, there are few channels with U bases (Figure 5.8).

The V shape channels are single and also consists of aggrading surfaces as well however, the architectural elements are same as the main channel erosional surface due to same stacking patterns (Figure 5.9) whereas, the U shape channel-04 have gentle bases with low angle as indicated on the dip map (Figure 5.10). The dip angle for the representative V shape channels i.e. (1 to 3) ranging from 2° to 30° whereas, for the U shape representative channel-04 the dip angle ranges from 1° to 11° (Figure 5.10). In addition, the channel shows discontinuous reflections at some points which indicate side wall collapses, and erosional effects (Figure 5.9).

The V shape channels are sharp and eroded especially in the distal area as compare to proximal area whereas, the U shape channel-levee is gentle from proximal to the distal area. Furthermore, the terraces are present more in V shape channels and identified by low to high seismic amplitudes (compared with the bases of channels) with parallel to sub-parallel reflections whereas, the terrace in U shape channel-04 is gentle with medium to high seismic amplitude. In addition, the V shape channels i.e. (1 to 3) have higher angle values whereas, the U shape channel-04 is gentle and lower angle value (Figure 5.9).
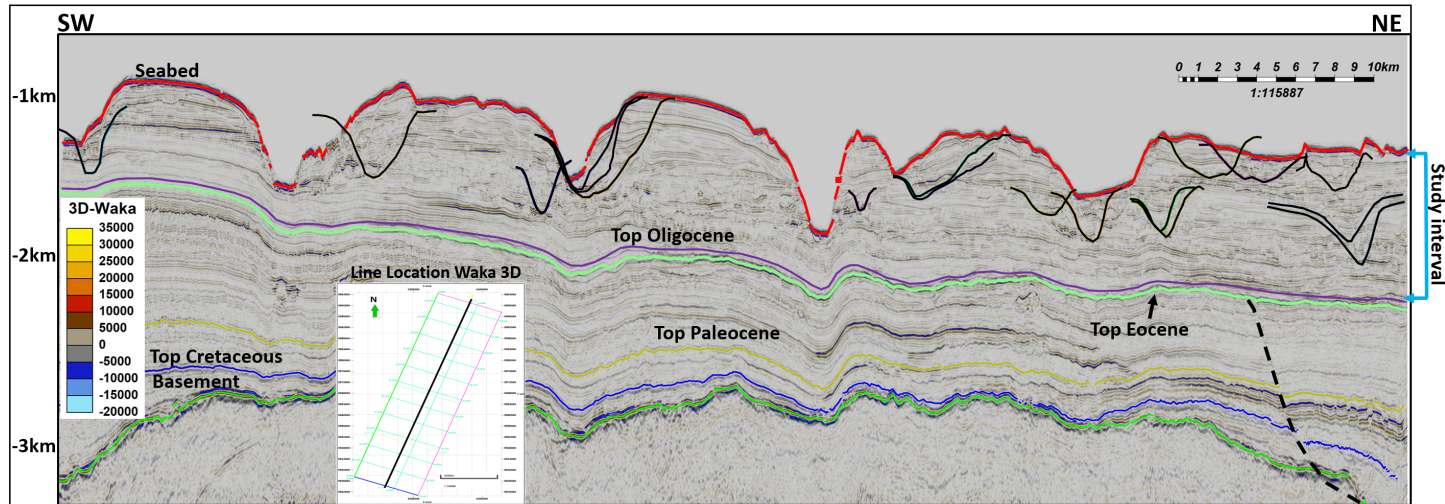
Figure 5.8: Incisions interpretation from Top Oligocene to Seabed Horizon in the study interval shown by black lines.

5.6.1 Architectural elements and facies analysis of the erosional surface (channels) and it's filling deposits

The main seismic architectural elements identified within the channels include conformable reflection elements, high amplitude reflection elements, massive low amplitude reflection elements furthermore, facies associated with channels are interpreted based on their reflection configuration of channel fills, the shape of erosional surfaces, stacking patterns and architectural elements. In addition, the amplitudes are low to high from proximal to distal area in the four types of representative channels (Figure 5.9). The channels i.e. (1 to 3) are aggrading and on-lapping on the Channel incision surface whereas, the channel-04 is just on-lapping on the channel incision surface and the continuity is medium to low. The low reflection amplitudes are mostly located in the bases of the channels system which are related to the first order stage for the channel development, and it is the erosional phase. The lateral distribution of sediments from proximal to the distal area is continuous and discontinuous when the channel starts aggrading (Figure 5.9).

Four types of seismic facies associated with channels are interpreted base on their reflection configuration of channels fills the shape of erosional surfaces, stacking patterns and architectural elements (Figure 5.9). In channel-1 the seismic facies are characterized by low to high amplitude, high continuity and parallel seismic reflections confined with the V-shaped erosional surface. Facies inside the channel-1 shows lateral and uniform fill reflection which is mostly on-lapping with the erosional surface and the exaggeration of the channel is in the vertical direction. Furthermore, the thickness and sequential development is complex and varying from the schematic shown in (Figure 5.9).

In channel-2 Seismic facies consist of parallel to subparallel seismic reflections, variable amplitude, and continuity with V shape erosional surface. Furthermore, the aggrading channels fills are present along the walls which depict that the channel is aggrading in the lateral direction and on-lapping on the channel erosional surface (Figure 5.9). Whereas, in channel-3 the seismic facies consist of subparallel seismic reflections, moderate amplitude and variable continuity with V shape erosional surface (Figure 5.9). In addition, the reflections are mostly on-lapping with the channel erosional surface (Figure 5.9) and deposits at the top of channel fill are more continuous and parallel as compared to the base deposits indicate different lithologies filling inside the channel surface (Figure 5.9). Furthermore, in channel-04 the Seismic facies consist of variable amplitude and continuity, subparallel to chaotic seismic reflections confined with U shaped erosional surface. In, addition at lower areas of channel slope the decrease in gradient indicates that the sediments are down-cutting with U-shape morphology and the reflections are mostly on-lapping with the channel erosional surface (Figure 5.9).
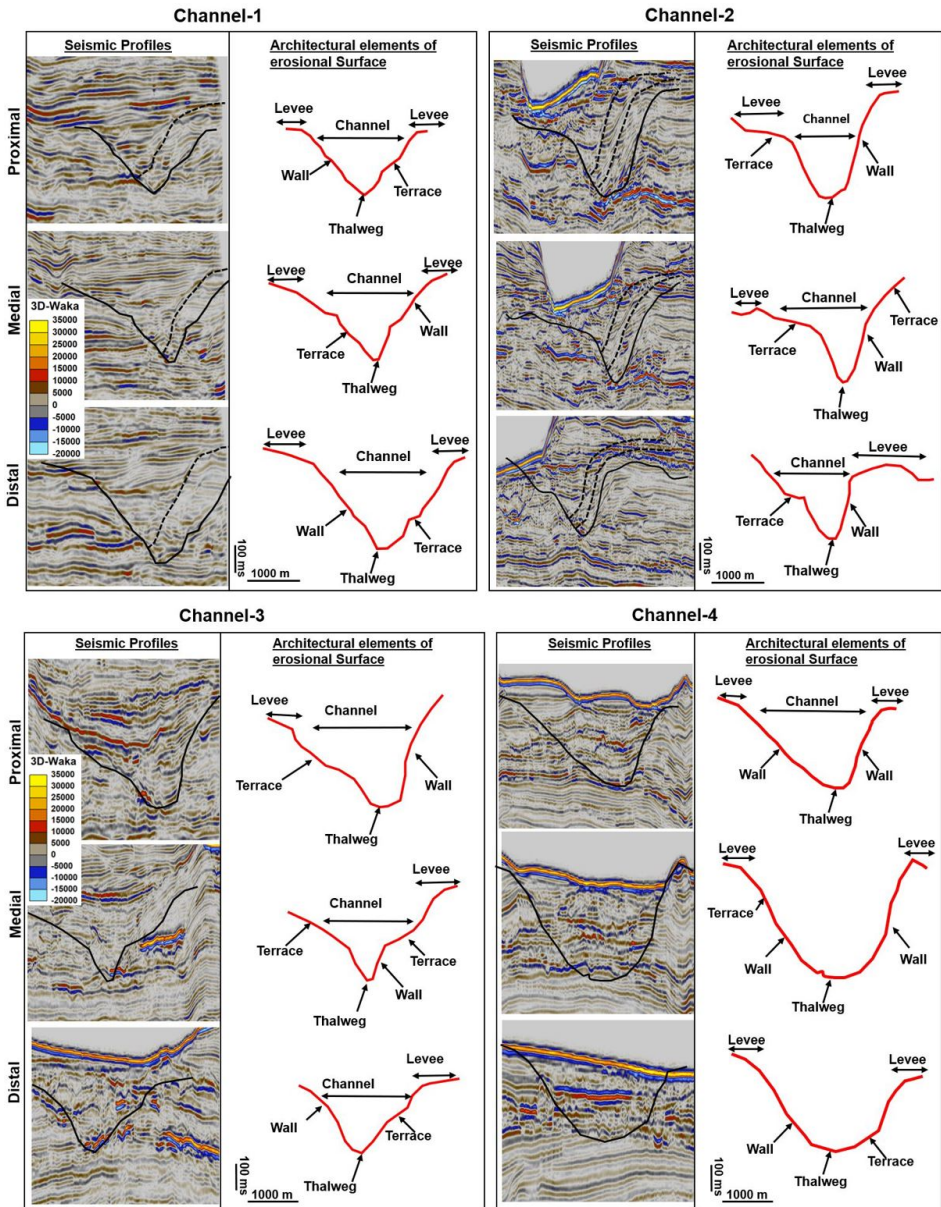
Figure 5.9: Seismic facies analysis of channels in the study area, representing the proximal-distal system.
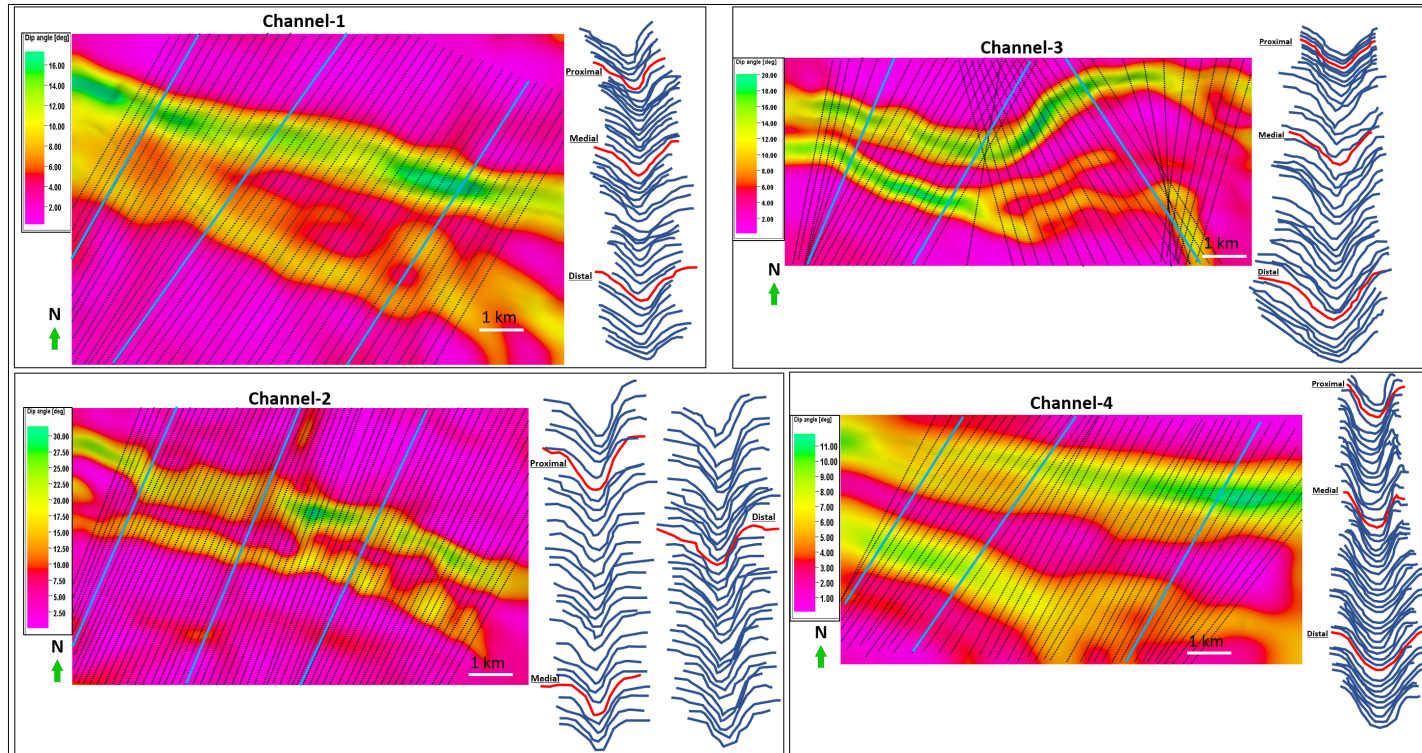
Figure 5.10: Morphometric analysis of channels with Dip-angle (degree) map of channels and locations of cross-sections (left images) with perpendicular channels cross-sections (right).

5.6.2 Quantitative morphometric analysis of Channels

Channels 1, 2 and 3 are having V shapes and at their proximal area, the morphology is dominated by steep walls with terraces. Whereas, in channel-04 having U shape morphology that consist of gentle walls and base (Figure 5.9). In addition, the channel-04 base at the proximal area is sharp and walls are steeper as compare to the distal area (Figure 5.9). The channels gradient increases towards the distal area (Figure 5.11, Table 5.1) as compared to the proximal area. The channels heights are approximately (140-400 m) from proximal to the medial area and (180-320 m) in the distal area with the increasing trend as compared to the distal area (Table 5.1, Figure 5.11).

The channel-01 and its tributaries having V shape morphology with a height range from (150 to 310 m) and the height decreases at the distal area. In addition, the top width ranges from (973 to 3066 m) and decreases at the distal area (Table 5.1, Figure 5.11). The cross-sectional areas (CSA) ranges from (0.01 to 0.10 km^2). Furthermore, the channel-01 and it's tributary 1b show higher cross-sectional areas (CSA) whereas, the tributary 1a shows lower values from proximal to distal areas (Table 5.1, Figure 5.11). The gradient ranges from (0.7 to 1.8) and it shows a linear trend for channel-01 and it's tributary 1b whereas, for tributary 1a the trend in nonlinear. In addition, the aspect ratio (width/height) ranges from (5.7 to 16.5) and it shows a linear trend from proximal to the distal area. Furthermore, the sinuosity is low for the tributaries 1a and 1b of channel-01 whereas, it is straight for the channel-01 (Table 5.1, Figure 5.11).

The channel-02 having V shape morphology with height ranges from (150 to 237 m) and the height range starts decreases at the distal area. In addition, the top width ranges from (4490 to 5838 m) and its values are largest in the representative channels of the study area (Table 5.1, Figure 5.11). The cross-sectional areas (CSA) ranges from (0.07 to 0.12 km^2) and the values decrease in the distal area (Table 5.1, Figure 5.11). The gradient ranges from (0.58 to 0.86) and it shows a linear trend from proximal to the distal area. In addition, the aspect ratio (width/height) ranges from (19 to 33) and it shows the highest values in the representative channels and further increases in the distal area. Furthermore, the sinuosity is straight from the proximal to medial areas whereas, it is higher in the distal area (Table 5.1, Figure 5.11).

The channel-03 and its tributaries having V shape morphology with a height range from (272 to 450 m) and the height range starts decreases at the distal area. In addition, the top width ranges from (2443 to 4340 m) and the range start decreases at the distal area (Table 5.1, Figure 5.11). The cross-sectional areas (CSA) ranges from (0.03 to 0.10 km^2). Furthermore, the tributaries (3a and 3b) show higher cross-sectional areas (CSA) as compare to channel-03 (Table 5.1, Figure 5.11). The gradient ranges from (1.4 to 3) and it shows a linear trend from proximal to medial area whereas it starts decreases towards the distal area. In addition, the aspect ratio (width/height) ranges from (6.3 to 12.8) and it shows a linear trend from proximal to the distal area. Furthermore, the sinuosity is straight from proximal to medial area whereas, it is low in the distal area (Table 5.1, Figure 5.11).
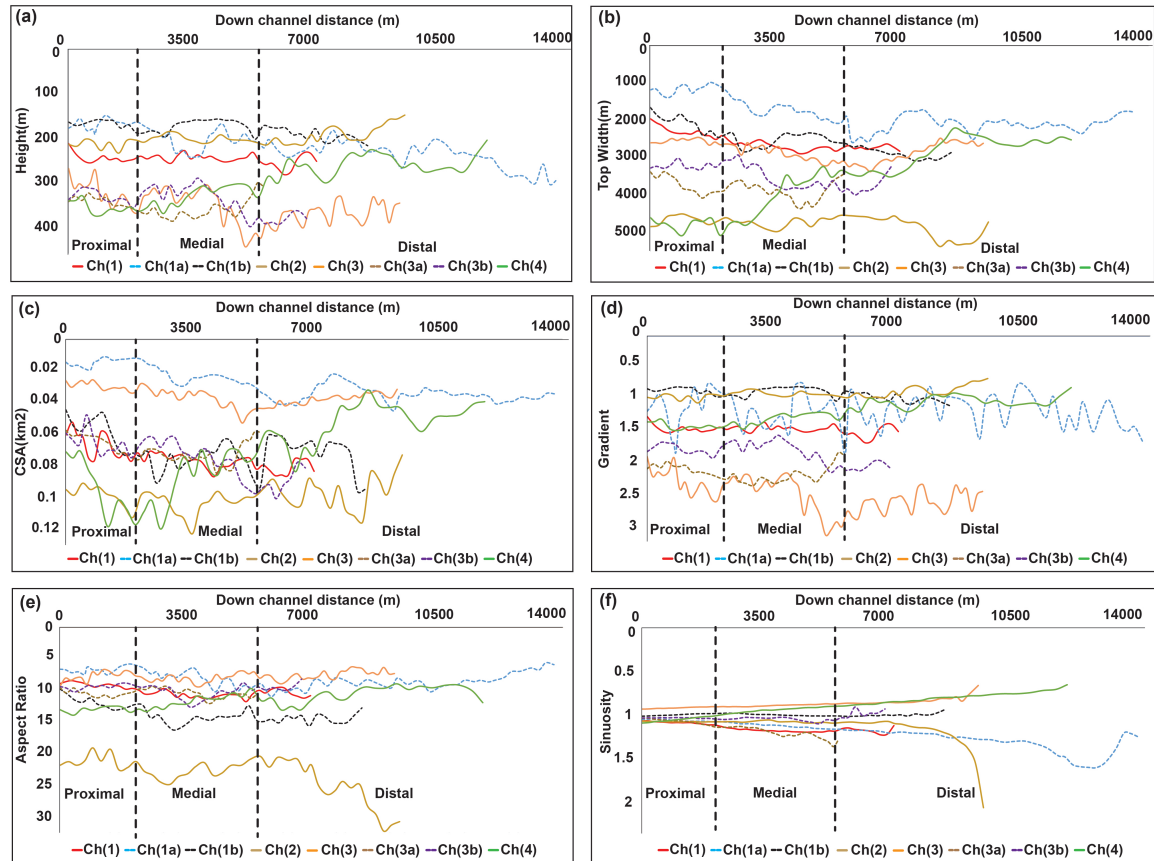
Figure 5.11: Morphometric analysis of channels. (a) Heights of channels vs. Distance. (b) Top width of channels vs. Distance. (c) Cross-sectional area of channels vs. Distance. (d) Gradients of channels vs. Distance. (e) Aspect ratio of channels vs. Distance. (f) Sinuosity of channels vs. Distance. Solid lines represent the main channel while the dashed lines represent the tributaries of the channels.

The channel-04 having U shape morphology with height ranges from (207 to 380 m) and the height range starts decreases at the distal area. In addition, the top width ranges from (2195 to 5068 m) decreases towards the distal area (Table 5.1, Figure 5.11). The cross-sectional areas (CSA) ranges from (0.03 to 0.12 km^2) and the values decrease in the distal area (Table 5.1, Figure 5.11). The gradient ranges from (0.65 to 1.73) and it shows a linear trend from proximal to the distal area but the values start decreasing towards the distal area. In addition, the aspect ratio (width/height) ranges from (9.07 to 14.13) and it shows a linear trend from proximal to the distal area. Furthermore, the sinuosity is low from proximal to the distal area (Table 5.1, Figure 5.11).

	Height (m)			Width Average (m)			Top Width (m)			CSA (km^2)			Linear Equation
	Max	Min	Avg	Top	base	Ratio	Max	Min	Avg	Max	Min	Avg	Distance vs Height
Channels													
1	308	151	229.5	1805	343	0.19	2564	973	1805	0.05	0.01	0.03	y = 0.0019x + 243.74
1a	286	215	250.5	2563	400	0.16	2877	1944	2563	0.09	0.05	0.08	y = 0.0076x + 170.89
1b	220	160	190	2531	348	0.14	3066	1644	2531	0.10	0.05	0.07	y = 0.0044x + 162.61
2	237	150	201	4788	704	0.15	5838	4490	4788	0.12	0.07	0.10	y = -0.004x + 220.91
3	450	272	361	2798	585	0.21	3359	2443	2798	0.05	0.03	0.04	y = 0.0074x + 323.76
3a	386	305	345.5	3810	531	0.14	4340	3360	3810	0.09	0.06	0.07	y = 0.0009x + 355.76
3b	405	294	349.5	3470	357	0.10	3980	2919	3470	0.10	0.05	0.08	y = 0.0101x + 312.97
4	380	207	293.5	3582	405	0.11	5068	2195	3582	0.12	0.03	0.07	y = -0.0122x + 371.72

	Sinuosity			Gradient			Aspect ratio (width/height)			Height (m)		Top width (m)	
	Max	Min	Avg	Max	Min	Avg	Max	Min	Avg	R^2	R	R^2	R
Channels													
1	1.56	1.02	1.18	1.77	0.71	1.14	11.13	5.67	8.19	0.68	0.82	0.71	0.84
1a	1.19	1.04	1.12	1.64	1.16	1.41	11.96	8.56	10.25	0.11	0.33	0.51	0.71
1b	0.99	0.91	0.97	1.05	0.76	0.86	16.54	9.90	13.96	0.40	0.64	0.74	0.86
2	2.00	1.03	1.11	1.08	0.58	0.86	32.91	19.44	24.00	0.39	0.62	0.26	0.51
3	0.91	0.64	0.85	3.00	1.81	2.39	9.54	6.34	7.86	0.29	0.53	0.08	0.28
3a	1.32	1.01	1.13	2.55	1.67	2.07	12.19	9.46	10.65	0.00	0.07	0.13	0.37
3b	1.07	0.88	1.00	2.30	1.40	1.72	12.86	8.29	10.05	0.42	0.65	0.51	0.72
4	1.06	0.64	0.87	1.73	0.65	1.17	14.13	9.07	11.63	0.78	0.88	0.89	0.94

Table 5.1: Summary of morphometry data for four channels including its tributaries.

Chapter 6

Discussion

6.1 Development of Submarine Channels

The Canterbury basin evolution from mid-Cretaceous to the present day sedimentary succession is divided into three main phases. The first phase occurred in the mid-Cretaceous to late-Cretaceous, where syn-rift fault system was pronounced in the Canterbury basin and these faults were associated with the syn-rift sedimentation (O'Leary and Mogg, 2008). The second phase occurred in the late-Cretaceous to Oligocene, where the basin was largely tectonically quiescent and marine transgression occurred during thermal subsidence (Mogg et al., 2008). The third phase was characterized by Neogene foreset progradation where the regression was dominant. Furthermore, the southern Alps uplifted with a new source of clastics emerged and the deposition was strongly regressive in the Miocene time (O'Leary and Mogg, 2008).

Seismic facies, attribute and morphological analysis on the study interval also revealed some complex of incisions with V and U shaped, isolated bright amplitude with relatively non-linear correlation on the morphometric scaling relationship (Figure 5.6, Figure 5.7, Figure 5.9, Figure 5.10, and Figure 6.1) that indicated a submarine channels (sensu Hajek et al., 2010; Hofmann et al., 2011; Posamentier and Kolla, 2003; Kolla et al., 2007; Jobe et al., 2016). In addition, the Submarine Channels interpreted in Waka-3D seismic reflection survey (Figure 5.8, Figure 6.1) shows that the submarine channels are present from Oligocene to Seabed which is the Study interval for thesis work. The inception of Channels was interpreted to be early Oligocene by Sahoo et al. (2015). Furthermore, Lever (2007) postulated that unconformities in the shallow water successions within the Oligocene may have been caused by global sea level falls and sub-Antarctic oceanic current activities (Miller et al., 2005). Sediment failures and gravity flows were common during the evolution of unidirectional migrating deep water Submarine Channels (Gong et al., 2013) and the evidence of unidirectional Submarine Channels observed on the seismic profiles for

the representative channels (Figure 5.9).

The first stage of channel development (erosional surface) can be related to the massive low amplitude reflections which are located at the base of channels (Figure 5.9). In addition, these lateral shifting and vertically aggrading channel styles may occur in a variety of combinations, amalgamated or separated by erosional cuts or thick shales (Kolla and Coumes, 1987). Furthermore, the representative Submarine Channels in the study interval has an average height that ranges from 190 to 361 m and the width ranges from 1805 to 4788 m (Table 5.1) which indicate more deposition and late stage of filling after the channels were build up due to prograding foresets (Miocene to recent) and increase of sedimentation supply in the second stage due to strike-slip movement along the Alpine fault (sensu Fulthorpe and Carter, 1991).

The channel stacking pattern indicates an increase in the gradient values (up to 3) and sediments are down cuttings with the superposition direction of Submarine Channels deposition which shows more erosional behavior as compare to depositional in the channel settings (Figure 5.9). At the proximal area the straight channel sinuosity indicates that the less flow of frequency increases with time as suggested by Gee et al. (2007) & Maier et al. (2013) and shown in Figure 5.11. Furthermore, at the proximal areas of the channels, the reflection terminations are mostly on-lapping, with chaotic & subparallel reflection configurations and low to medium amplitude values (Figure 5.9). In addition, at the medial area, the low sinuosity indicates the decrease in flow energy and erosive power downslope, however, it is difficult to evaluate the relationship between sediment supply and channel sinuosity without sediment supply as explained by Babonneau et al. (2002) and shown in Figure 5.11. Furthermore, at the medial areas of the channels, the reflection terminations are mostly on-lapping, with parallel to subparallel & chaotic reflection configurations and low to medium amplitude values (Figure 5.9). The distal area shows higher sinuosity values due to the channel sinuosity increases with time, and the meander cut-offs forming as explained by (Deptuck et al., 2003; Wynn et al., 2007; Gee et al., 2007; Maier et al., 2013) and shown in the Figure 5.11. Moreover, at the distal areas of channels the reflection terminations are on-lapping and down-lapping with the erosional surface, plus chaotic to subparallel reflection configurations and low to high amplitude values (Figure 5.9).

6.2 Implications of the submarine channels morphologies for palaeoenvironment reconstruction

The increase in height, width and cross-sectional area of the representative submarine channels with their morphologies and architecture (Figure 5.9) reveal spatial variations as erosion and backstepping of the shoreline occurred. Furthermore, the increase in morphometric parameters from proximal to the distal area also depict that the channel movement is facilitated by gravity, and the net transport from these currents are largely in seaward direction (Shepard and Marshall, 1973; Shepard et al., 1974; Shepard, 1981). The presence of submarine channels in the study interval (Figure 5.8, Figure 6.1) indicating that they are good sediment conduits (Posamentier and Kolla, 2003; Stow and Mayall, 2000).

The stability of U shape submarine channels and morphologies indicate that the extended process involving in fine-grained sediments that can be carried over the shelf and upper slope into the submarine channels heads without significant erosion for example Posamentier (2003); Lonergan et al. (2013); Jobe et al. (2011). The Channels (3 & 4) with low sinuosities (Table 5.1, Figure 5.11) indicate that they were created by extended processes with flow energy (Posamentier and Kolla, 2003; Shepard and Marshall, 1973; Wynn et al., 2007). Furthermore, the thalweg of the initial channels may have been eroded due to subsequent gravity flows as depicted in Figure 5.9 during the superposition process, and its inner bank is usually preserved lateral migration.

The lateral displacement of channel banks indicates the lateral migration of the channel systems in the study area (Figure 5.9). The submarine channels gradient is considered to be a major control on turbidity-current behaviour (Babonneau et al., 2002; McHargue et al., 2011; Stevenson et al., 2013). Furthermore, in the study area the correlations between decreasing channel gradients and widened channel floors have been observed in the distal area of the channel axis (Figure 5.11, Figure 5.9). In addition, these correlations are consistent with results from previous studies by (Babonneau et al., 2002). Apart from widened channel floors, decreases in channel gradient could also lead to reduced flow energy, sediment deposition, widened submarine channels and decreased channel heights (e.g. Adeogba et al., 2005; Estrada et al., 2005). The amplitude and continuity variations inside the channels indicate that they have different origin and the channel deposits are accumulated in a channel abandonment stage as previously explained by Deptuck et al. (2003). Furthermore, the vertical and lateral superposition is due to the increase of gradient (Fu et al., 2019).

6.3 Implication for hydrocarbon prospectivity in the study area

The interconnections between the sediment conduits and their products such as submarine channels can be considered as implications for hydrocarbon prospectivity in the study area and similar basins worldwide. In the study area, low amplitude and continuous reflection elements (Figure 5.9, Figure 6.1) indicate that the channels are mostly filled with a fine-grained material that could possibly act as a reservoir and source rocks (Bouma, 2000, 2001; Sutherland and Browne, 2003; Uruski, 2010). The High amplitude reflections above the low amplitude reflections package in representative channels (Figure 5.9, Figure 6.1) depict the presence of coarse-grained sediments caused by erosive energetic flows (Jobe et al., 2011) that could form good hydrocarbon reservoirs. In addition, the conformable reflection elements at the top of the channel fill could provide potential seal rock (Figure 5.9). Furthermore, in terms of volume, significant amounts of reservoir volume are also achievable from channels in the study area, as indicated by the high values (0.12) of cross-sectional area (Figure 5.11, Table 5.1).
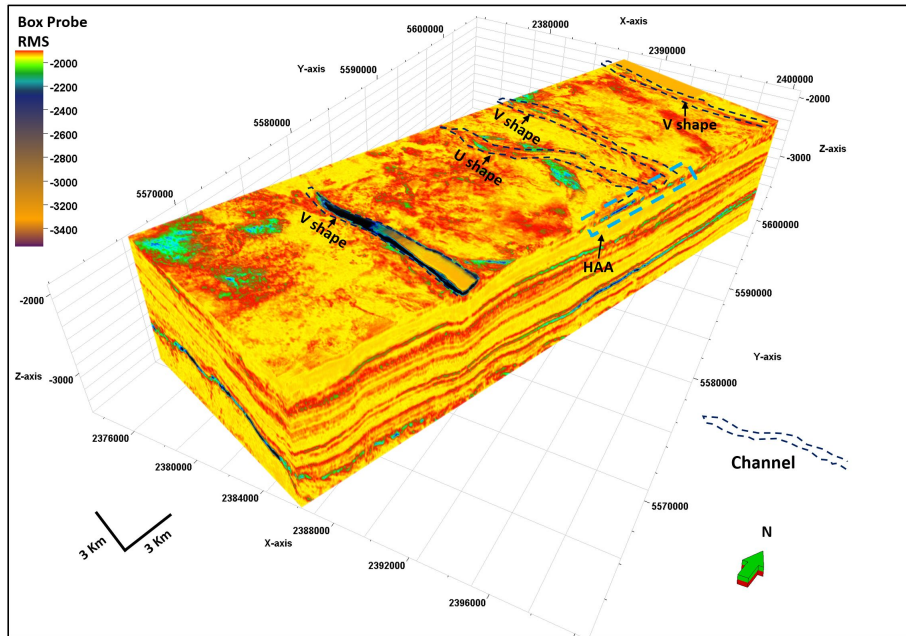
Figure 6.1: RMS Amplitude cube represents the channel system and its RMS Amplitude variation in the study area.

6.4 Morphometry comparison with other sediment conduit systems

The channels in the study area have heights that range from 190 to 361 m (Figure 6.2, Table 5.1) and are comparable to other channels documented by (Qin et al., 2016; Gamboa et al., 2012) on Esprito Santo Basin (SE Brazil) and (Harishidayat et al., 2018) on Barent sea. Furthermore, the channels average width in the study area ranges from 1805 to 4788 m (Figure 6.2, Table 5.1), whereas, those reported in the work of (Qin et al., 2016; Gamboa et al., 2012; Harishidayat et al., 2018) are relatively less wide. These differences are may be due to the flow properties, for example, grain size distribution, flow volume and fluid saturation (sensu Qin et al., 2016; Shepard and Marshall, 1973; Babonneau et al., 2004). In addition, Qin et al. (2016) work measure the complete channel system but this thesis study data is in a small portion of the long submarine channel system in Canterbury basin (Figure 6.2, Figure 2.1).

Figure 6.2: Morphometry comparison of Channel system on the study area with Qin et al. (2016); Gamboa et al. (2012); Harishidayat et al. (2018) on the canyon system.

Chapter 7

Conclusions

The following are the main conclusions from this work.

- The channels in the study area can be categorized as Four main types based on their reflection configuration of channels fills, the shape of erosional surfaces, stacking patterns and architectural elements.

- Channels are the predominant sediment conduits in the study area and formed during deep-marine environment on the Oligocene to Recent.

- Seismic facies and morphometry analysis of Channels in the study area revealed that channels are potential to become hydrocarbon reservoir and its deep-marine system supported the presences of source rocks, seal rocks and stratigraphic traps.

- The geometry of the submarine channels in the study area is comparable to other submarine channels observed worldwide. However, spatial and temporal variations suggest the role of local factors (e.g. levee collapse, tributaries, salt diapirs) on its development and later evolution.

- The morphometric analysis of sediment conduits in the study area played an important role in the quantitative interpretation of the related sedimentary processes and paleoenvironment. Thus, it's applicable to a similar setting worldwide.

Bibliography

Abreu, V., Sullivan, M., Pirmez, C., Mohrig, D., 2003. Lateral accretion packages (laps): an important reservoir element in deep water sinuous channels. Marine and Petroleum Geology 20 (6-8), 631–648.

Adeogba, A. A., McHargue, T. R., Graham, S. A., 2005. Transient fan architecture and depositional controls from near-surface 3-d seismic data, niger delta continental slope. AAPG bulletin 89 (5), 627–643.

Anderson, P., Newrick, R., 2008. Strange but true stories of synthetic seismograms. CSEG Recorder 12 (December), 51–56.

Arnott, R., 2007. Stratal architecture and origin of lateral accretion deposits (lads) and conterminuous inner-bank levee deposits in a base-of-slope sinuous channel, lower isaac formation (neoproterozoic), east-central british columbia, canada. Marine and Petroleum Geology 24 (6-9), 515–528.

Avseth, P., Mukerji, T., Mavko, G., 2005. Common techniques for quantitative seismic interpretation. Cambridge University Press, p. 168257.

Babonneau, N., Savoye, B., Cremer, M., Bez, M., 2004. Multiple terraces within the deep incised zaire valley (zaïango project): are they confined levees? Geological Society, London, Special Publications 222 (1), 91–114.

Babonneau, N., Savoye, B., Cremer, M., Klein, B., 2002. Morphology and architecture of the present canyon and channel system of the zaire deep-sea fan. Marine and Petroleum Geology 19 (4), 445–467.

Badley, M. E., 1985. Practical seismic interpretation.

Bain, H. A., Hubbard, S. M., 2016. Stratigraphic evolution of a long-lived submarine channel system in the late cretaceous nanaimo group, british columbia, canada. Sedimentary geology : international journal of applied and regional sedimentary 337, 113–132.

Ballance, P., 1992. New Zealand geology: an illustrated guide. Geoscience Society of New Zealand.

Bouma, A., 2001. Geological architecture and reservoir characteristics of fine-grained and coarse-grained turbidite systems.

Bouma, A. H., 2000. Coarse-grained and fine-grained turbidite systems as end member models: applicability and dangers. Marine and Petroleum Geology 17 (2), 137–143.

Bouma, A. H., 2004. Key controls on the characteristics of turbidite systems. Geological Society, London, Special Publications 222 (1), 9–22.

Brown, A. R., 2004. Interpretation of three-dimensional seismic data (vol. 42). tulsa, okla. American Association of Petroleum Geologists.

Brown, A. R., 2005. Pitfalls in 3d seismic interpretation: Keynote presentation at the 11th annual 3-d seismic symposium, denver. The Leading Edge 24 (7), 716–717.

Browne, G., Field, B., 1988. A review of cretaceous-cenozoic sedimentation and tectonics, east coast, south island, new zealand.

Cameron, M., Fomel, S., Sethian, J., 2008. Time-to-depth conversion and seismic velocity estimation using time-migration velocity. Geophysics 73 (5), VE205–VE210.

Campbell, H., Malahoff, A., Browne, G., Graham, I., Sutherland, R., 2012. New zealand geology. Episodes 35 (1), 57–71.

Campion, K. M., Sprague, A., Mohrig, D., Lovell, R., Drzewiecki, P., Sullivan, M., Ardill, J., Jensen, G., Sickafoose, D., 2003. Outcrop expression of confined channel complexes.

Cande, S. C., Stock, J. M., 2004. Pacific-antarctic-australia motion and the formation of the macquarie plate. Geophysical journal international 157 (1), 399–414.

Cannon, S., 2018. 3.1.1 depth conversion, 52.
    URL   https://app.knovel.com/hotlink/khtml/id:kt011O717F/reservoir-modelling-practical/depth-conversion

Carter, R., 1988. Post-breakup stratigraphy of the kaikoura synthem (cretaceous-cenozoic), continental margin, southeastern new zealand. New Zealand journal of geology and geophysics 31 (4), 405–429.

Cartwright, J. A., 1994. Episodic basin-wide fluid expulsion from geopressured shale sequences in the north sea basin. Geology 22 (5), 447–450.

Catterall, V., Redfern, J., Gawthorpe, R., Hansen, D., Thomas, M., 2010. Architectural style and quantification of a submarine channel–levee system located in a structurally complex area: offshore nile delta. Journal of Sedimentary Research 80 (11), 991–1017.

Chopra, S., Marfurt, K. J., 2005. Seismic attributesa historical perspective. Geophysics 70 (5), 3SO–28SO.

Chough, S., Hesse, R., 1976. Submarine meandering thalweg and turbidity, currents flowing for 4,000 km in the, northwest atlantic mid-ocean channel, labrador sea. Geology 4 (9).

Clark, I. R., Cartwright, J. A., 2011. Key controls on submarine channel development in structurally active settings. Marine and Petroleum Geology 28 (7), 1333 – 1349.
URL http://www.sciencedirect.com/science/article/pii/S0264817211000572

Clark, J., Kenyon, N., Pickering, K., 1992. Quantitative analysis of the geometry of submarine channels: implications for the classification of submarine fans. Geology 20 (7), 633–636.

Clark, J. D., Pickering, K. T., 1996. Architectural elements and growth patterns of submarine channels: application to hydrocarbon exploration. AAPG bulletin 80 (2), 194–220.

Cook, R. A., Sutherland, R., Zhu, H., 1999. Cretaceous-Cenozoic Geology and Petroleum Systems of the Great South Basin, New Zealand. Vol. 20. Institute of Geological & Nuclear Sciences.

Cooper, A. F., Barreiro, B. A., Kimbrough, D., Mattinson, J. M., 1987. Lamprophyre dike intrusion and the age of the alpine fault, new zealand. Geology 15 (10).

Cronin, B., Owen, D., Hartley, A., Kneller, B., 1998. Slumps, debris flows and sandy deep-water channel systems: implications for the application of sequence stratigraphy to deep water clastic sediments. Journal of the Geological Society 155 (3), 429–432.

Cronin, B. T., Akhmetzhanov, A. M., Mazzini, A., Akhmanov, G., Ivanov, M., Kenyon, N. H., et al., 2005. Morphology, evolution and fill: implications for sand and mud distribution in filling deep-water canyons and slope channel complexes. Sedimentary Geology 179 (1-2), 71–97.

Damuth, J. E., Kowsmann, R. O., Flood, R. D., Belderson, R. H., Gorini, M. A., 1983. Age relationships of distributary channels on amazon deep-sea fan: implications for fan growth pattern. Geology 11 (8), 470–473.

Davey, F., Bennett, D., Houtz, R., 1982. Sedimentary basins of the ross sea, antarctica. New Zealand Journal of Geology and Geophysics 25 (2), 245–255.

Deptuck, M. E., Steffens, G. S., Barton, M., Pirmez, C., 2003. Architecture and evolution of upper fan channel-belts on the niger delta slope and in the arabian sea. Marine and Petroleum Geology 20 (6-8), 649–676.

Deptuck, M. E., Sylvester, Z., Pirmez, C., OByrne, C., 2007. Migration–aggradation history and 3-d seismic geomorphology of submarine channels in the pleistocene benin-major canyon, western niger delta slope. Marine and Petroleum Geology 24 (6-9), 406–433.

Di Celma, C. N., Brunt, R. L., Hodgson, D. M., Flint, S. S., Kavanagh, J. P., 2011. Spatial and temporal evolution of a permian submarine slope channel–levee system, karoo basin, south africa. Journal of Sedimentary Research 81 (8), 579–599.

Dugan, B., Sheahan, T., 2012. Offshore sediment overpressures of passive margins: Mechanisms, measurement, and models. Reviews of Geophysics 50 (3).

Estrada, F., Ercilla, G., Alonso, B., 2005. Quantitative study of a magdalena submarine channel (caribbean sea): implications for sedimentary dynamics. Marine and Petroleum Geology 22 (5), 623–635.

Falkowski, T., Ostrowski, P., Bogucki, M., Karczmarz, D., 2018. The trends in the main thalweg path of selected reaches of the middle vistula river, and their relationships to the geological structure of river channel zone. Open Geosciences 10 (1), 554–564.

Fu, C., Yu, X., Dong, Y., He, Y., Liang, J., Kuang, Z., 2019. Sedimentary characteristics comparison and genesis analysis of the deepwater channel in the hydrate enrichment zones on the north slope of the south china sea. Acta Oceanologica Sinica 38 (3), 103–113.

Fulthorpe, C. S., Carter, R. M., 1991. Continental-shelf progradation by sediment-drift accretion. Geological Society of America Bulletin 103 (2), 300–309.

Fulthorpe, C. S., Carter, R. M., Miller, K. G., Wilson, J., 1996. Marshall paraconformity: a mid-oligocene record of inception of the antarctic circumpolar current and coeval glacio-eustatic lowstand? Marine and petroleum geology 13 (1), 61–77.

Gaina, C., Müller, D. R., Royer, J.-Y., Stock, J., Hardebeck, J., Symonds, P., 1998. The tectonic history of the tasman sea: a puzzle with 13 pieces. Journal of Geophysical Research: Solid Earth 103 (B6), 12413–12433.

Gamberi, F., Rovere, M., Dykstra, M., Kane, I. A., Kneller, B. C., 2013. Integrating modern seafloor and outcrop data in the analysis of slope channel architecture and fill. Marine and Petroleum Geology 41, 83–103.

Gamboa, D., Alves, T. M., 2015. Spatial and dimensional relationships of submarine slope architectural elements: a seismic-scale analysis from the espírito santo basin (se brazil). Marine and Petroleum Geology 64, 43–57.

Gamboa, D., Alves, T. M., Cartwright, J., 2012. A submarine channel confluence classification for topographically confined slopes. Marine and Petroleum Geology 35 (1), 176–189.

Gardner, G., Gardner, L., Gregory, A., 1974. Formation velocity and densitythe diagnostic basics for stratigraphic traps. Geophysics 39 (6), 770–780.

Gardner, M. H., Borer, J. M., 2000. Aapg memoir 72/sepm special publication no. 68, chapter 19: Submarine channel architecture along a slope to basin profile, brushy canyon formation, west texas.

Gardner, M. H., Borer, J. M., Melick, J. J., Mavilla, N., Dechesne, M., Wagerle, R. N., 2003. Stratigraphic process-response model for submarine channels and related features from studies of permian brushy canyon outcrops, west texas. Marine and Petroleum Geology 20 (6-8), 757–787.

Gee, M., Gawthorpe, R., Bakke, K., Friedmann, S., 2007. Seismic geomorphology and evolution of submarine channels from the angolan continental margin. Journal of Sedimentary Research 77 (5), 433–446.

Gong, C., Wang, Y., Zhu, W., Li, W., Xu, Q., 2013. Upper miocene to quaternary unidirectionally migrating deep-water channels in the pearl river mouth basin, northern south china sea. AAPG bulletin 97 (2), 285–308.

Grecula, M., Flint, S. S., Wickens, H. D. V., Johnson, S. D., 2003. Upward-thickening patterns and lateral continuity of permian sand-rich turbidite channel fills, laingsburg karoo, south africa. Sedimentology 50 (5), 831–853.

Hajek, E. A., Heller, P. L., Sheets, B. A., 2010. Significance of channel-belt clustering in alluvial basins. Geology 38 (6), 535–538.

Hansen, L., Janocko, M., Kane, I., Kneller, B., 2017. Submarine channel evolution, terrace development, and preservation of intra-channel thin-bedded turbidites: Mahin and avon channels, offshore nigeria. Marine Geology 383, 146–167.

Hansen, L. A., Callow, R. H., Kane, I. A., Gamberi, F., Rovere, M., Cronin, B. T., Kneller, B. C., 2015. Genesis and character of thin-bedded turbidites associated with submarine channels. Marine and Petroleum Geology 67, 852–879.

Harishidayat, D., Omosanya, K. O., Johansen, S. E., Eruteya, O. E., Niyazi, Y., 2018. Morphometric analysis of sediment conduits on a bathymetric high: Implications for palaeoenvironment and hydrocarbon prospectivity. Basin Research 30 (5), 1015–1041.

Hart, B. S., 2011. An introduction to seismic interpretation. American Association of Petroleum Geologists, p.224.

Hofmann, M. H., Wroblewski, A., Boyd, R., 2011. Mechanisms controlling the clustering of fluvial channels and the compensational stacking of cluster belts. Journal of Sedimentary Research 81 (9), 670–685.

James, G., Witten, D., Hastie, T., Tibshirani, R., 2013. An introduction to statistical learning. Vol. 112. Springer.

Janocko, M., Nemec, W., Henriksen, S., Warchoł, M., 2013. The diversity of deep-water sinuous channel belts and slope valley-fill complexes. Marine and Petroleum Geology 41, 7–34.

Jobe, Z. R., Howes, N. C., Auchter, N. C., 2016. Comparing submarine and fluvial channel kinematics: Implications for stratigraphic architecture. Geology 44 (11), 931–934.

Jobe, Z. R., Lowe, D. R., Uchytil, S. J., 2011. Two fundamentally different types of submarine canyons along the continental margin of equatorial guinea. Marine and Petroleum Geology 28 (3), 843–860.

Jolly, B. A., Lonergan, L., Whittaker, A. C., 2016. Growth history of fault-related folds and interaction with seabed channels in the toe-thrust region of the deep-water niger delta. Marine and Petroleum Geology 70, 58 – 76.
URL http://www.sciencedirect.com/science/article/pii/S0264817215301276

Kane, I. A., Hodgson, D. M., 2011. Sedimentological criteria to differentiate submarine channel levee subenvironments: exhumed examples from the rosario fm.(upper cre-

taceous) of baja california, mexico, and the fort brown fm.(permian), karoo basin, s. africa. Marine and Petroleum Geology 28 (3), 807–823.

Kim, Y. C., Hurt Jr, W. B., Maher, L. J., Starich, P. J., 1997. Hybrid migration: A cost-effective 3-d depth-imaging technique. Geophysics 62 (2), 568–576.

King, P. R., 2000. Tectonic reconstructions of new zealand: 40 ma to the present. New Zealand Journal of Geology and Geophysics 43 (4), 611–638.

Kolla, V., 2007. A review of sinuous channel avulsion patterns in some major deep-sea fans and factors controlling them. Marine and Petroleum Geology 24 (6-9), 450–469.

Kolla, V., Bourges, P., Urruty, J.-M., Safa, P., 2001. Evolution of deep-water tertiary sinuous channels offshore angola (west africa) and implications for reservoir architecture. AAPG bulletin 85 (8), 1373–1405.

Kolla, V., Coumes, F., 1987. Morphology, internal structure, seismic stratigraphy, and sedimentation of indus fan. AAPG Bulletin 71 (6), 650–677.

Kolla, V., Posamentier, H., Wood, L., 2007. Deep-water and fluvial sinuous channelscharacteristics, similarities and dissimilarities, and modes of formation. Marine and Petroleum Geology 24 (6-9), 388–405.

Koson, S., Chenrai, P., Choowong, M., 2014. Seismic attributes and their applications in seismic geomorphology. Bulletin of Earth Sciences of Thailand 6 (1), 1–9.

Lever, H., 2007. Review of unconformities in the late eocene to early miocene successions of the south island, new zealand: ages, correlations, and causes. New Zealand Journal of Geology and Geophysics 50 (3), 245–261.

Li, M., Zhao, Y., 2014. Chapter 4 - visualization and spectral decomposition, 75 – 102.
URL   http://www.sciencedirect.com/science/article/pii/B9780124104365000046

Lin, Y., Zhang, T., Liu, K. H., Gao, S. S., 2018. Identification of a shelf-edge submarine canyon using seismic attributes and spectral decomposition in the central gulf coast region of texas. In: SEG Technical Program Expanded Abstracts 2018. Society of Exploration Geophysicists, pp. 1748–1752.

Lonergan, L., Cartwright, J., Jolly, R., 1998. The geometry of polygonal fault systems in tertiary mudrocks of the north sea. Journal of Structural Geology 20 (5), 529–548.

Lonergan, L., Jamin, N. H., Jackson, C. A.-L., Johnson, H. D., 2013. U-shaped slope gully systems and sediment waves on the passive margin of gabon (west africa). Marine Geology 337, 80–97.

Macauley, R. V., Hubbard, S. M., 2013. Slope channel sedimentary processes and stratigraphic stacking, cretaceous tres pasos formation slope system, chilean patagonia. Marine and Petroleum Geology 41, 146 – 162, special Issue: Internal architecture, bedforms and geometry of turbidite channels.
URL   http://www.sciencedirect.com/science/article/pii/S0264817212000384

Maier, K. L., Fildani, A., McHargue, T. R., Paull, C. K., Graham, S. A., Caress, D. W., 2012. Punctuated deep-water channel migration: high-resolution subsurface data from the lucia chica channel system, offshore california, usa. Journal of Sedimentary Research 82 (1), 1–8.

Maier, K. L., Fildani, A., Paull, C. K., McHargue, T. R., Graham, S. A., Caress, D. W., 2013. Deep-sea channel evolution and stratigraphic architecture from inception to abandonment from high-resolution autonomous underwater vehicle surveys offshore central california. Sedimentology 60 (4), 935–960.

Marfurt, K. J., Alves, T. M., 2015. Pitfalls and limitations in seismic attribute interpretation of tectonic features. Interpretation 3 (1), SB5–SB15.

Marfurt, K. J., Kirlin, R. L., Farmer, S. L., Bahorich, M. S., 1998. 3-d seismic attributes using a semblance-based coherency algorithm. Geophysics 63 (4), 1150–1165.

Mayall, M., Jones, E., Casey, M., 2006. Turbidite channel reservoirskey elements in facies prediction and effective development. Marine and Petroleum Geology 23 (8), 821–841.

Mayall, M., Stewart, I., 2000. The architecture of turbidite slope channels. In: Deep-Water Reservoirs of the World: SEPM, Gulf Coast Section, 20th Annual Research Conference. Vol. 578. p. 586.

McHargue, T., E. Webb, J., 02 1986. Internal geometry, seismic facies, and petroleum potential of canyons and inner fan channels of the indus submarine fan. American Association of Petroleum Geologists Bulletin 70.

McHargue, T., Pyrcz, M. J., Sullivan, M. D., Clark, J., Fildani, A., Romans, B., Covault, J., Levy, M., Posamentier, H., Drinkwater, N., 2011. Architecture of turbidite channel systems on the continental slope: patterns and predictions. Marine and Petroleum Geology 28 (3), 728–743.

Miall, A. D., 1989. Architectural elements and bounding surfaces in channelized clastic deposits: Notes on comparisons between fluvial and turbidite systems. Sedimentary Facies in the Active Plate Margin. Edited by A. Taira and F. Masuda. TERRAPUB, Tokyo, 3–15.

Miller, K. G., Kominz, M. A., Browning, J. V., Wright, J. D., Mountain, G. S., Katz, M. E., Sugarman, P. J., Cramer, B. S., Christie-Blick, N., Pekar, S. F., 2005. The phanerozoic record of global sea-level change. science 310 (5752), 1293–1298.

Mitchum Jr, R. M., Vail, P. R., Sangree, J. B., 1977. Seismic stratigraphy and global changes of sea level: Part 6. stratigraphic interpretation of seismic reflection patterns in depositional sequences: Section 2. application of seismic reflection configuration to stratigraphic interpretation.

Mogg, W., Aurisch, K., O'Leary, R., Pass, G., 2008. The carrack-caravel prospect complex: a possible sleeping giant in the deep water canterbury basin, new zealand.

Mortimer, N., 2004. New zealand's geological foundations. Gondwana Research 7 (1), 261 – 272.

Mortimer, N., Campbell, H., 2014. Zealandia: Our continent revealed.

Mutti, E., Normark, W. R., 1987. Comparing examples of modern and ancient turbidite systems: problems and concepts. In: Marine clastic sedimentology. Springer, pp. 1–38.

Mutti, E., Normark, W. R., 1991. An integrated approach to the study of turbidite systems. In: Seismic facies and sedimentary processes of submarine fans and turbidite systems. Springer, pp. 75–106.

Mutti, E., Ricci Lucchi, F., 02 1978. Turbidites of the northern apennines: introduction to facies analysis. International Geology Review 20, 125–166.

Nakajima, T., Satoh, M., Okamura, Y., 1998. Channel-levee complexes, terminal deep-sea fan and sediment wave fields associated with the toyama deep-sea channel system in the japan sea. Marine Geology 147 (1-4), 25–41.

Noda, A., TuZino, T., Furukawa, R., Joshima, M., Uchida, J.-i., 2008. Physiographical and sedimentological characteristics of submarine canyons developed upon an active forearc slope: The kushiro submarine canyon, northern japan. Geological Society of America Bulletin 120 (5-6), 750–767.

Normark, W. R., Piper, D. J., Posamentier, H., Pirmez, C., Migeon, S., 2002. Variability in form and growth of sediment waves on turbidite channel levees. Marine Geology 192 (1-3), 23–58.

Normark, W. R., Posamentier, H., Mutti, E., 1993. Turbidite systems: state of the art and future directions. Reviews of Geophysics 31 (2), 91–116.

O'Leary, R., Mogg, W., 2008. The petroleum potential of the offshore canterbury basin: Insights from petroleum systems modelling.

Peakall, J., Wells, M. G., Cossu, R., Kane, I. A., Masson, D. G., Keevil, G. M., McCaffrey, W., Corney, R., 2013. Global (latitudinal) variation in submarine channel sinuosity: reply. Geology 41 (5), e288–e288.

Petroleum, N. Z., 2014. Minerals. new zealand petroleum basins; ministry of business. Innovation and Employment: Wellington, New Zealand, , pp. 38-105.

Pettinga, J. R., Yetton, M. D., Van Dissen, R. J., Downes, G., 2001. Earthquake source identification and characterisation for the canterbury region, south island, new zealand.

Pickering, K., Clark, J., Smith, R., Hiscott, R., Lucchi, F. R., Kenyon, N., 1995. Architectural element analysis of turbidite systems, and selected topical problems for sand-prone deep-water systems. In: Atlas of deep water environments. Springer, pp. 1–10.

Pigott, J. D., Kang, M.-H., Han, H.-C., 2013. First order seismic attributes for clastic seismic facies interpretation: Examples from the east china sea. Journal of Asian Earth Sciences 66, 34–54.

Piper, D. J., Normark, W. R., 1983. Turbidite depositional patterns and flow characteristics, navy submarine fan, california borderland. Sedimentology 30 (5), 681–694.

Posamentier, H., 2006. Deep-water turbidites and submarine fans. Facies models revisited, 397–520.

Posamentier, H. W., 2003. Depositional elements associated with a basin floor channel-levee system: case study from the gulf of mexico. Marine and Petroleum Geology 20 (6-8), 677–690.

Posamentier, H. W., Kolla, V., 2003. Seismic geomorphology and stratigraphy of depositional elements in deep-water settings. Journal of sedimentary research 73 (3), 367–388.

Pyles, D. R., Jennette, D. C., Tomasso, M., Beaubouef, R. T., Rossen, C., 2010. Concepts learned from a 3d outcrop of a sinuous slope channel complex: Beacon channel complex, brushy canyon formation, west texas, usa. Journal of Sedimentary Research 80 (1), 67–96.

Pyles, D. R., Tomasso, M., Jennette, D. C., 2012. Flow processes and sedimentation associated with erosion and filling of sinuous submarine channels. Geology 40 (2), 143–146.

Qin, Y., 2017. Geological controls on the evolution of submarine channels in the espírito santo basin, se brazil. Ph.D. thesis, Cardiff University.

Qin, Y., Alves, T. M., Constantine, J., Gamboa, D., 2016. Quantitative seismic geomorphology of a submarine channel system in se brazil (espírito santo basin): Scale comparison with other submarine channel systems. Marine and Petroleum Geology 78, 455–473.

Rafaelsen, B., 2006. Seismic resolution and frequency filtering. Univ. Tromso Lecture Series, Tromso, Norway.

Reimchen, A. P., Hubbard, S. M., Stright, L., Romans, B. W., 2016. Using sea-floor morphometrics to constrain stratigraphic models of sinuous submarine channel systems. Marine and Petroleum Geology 77, 92–115.

Sahoo, T. R., Browne, G. H., Hill, M. G., 2014. Seismic attribute analysis and depositional elements in the canterbury basin. In: Poster presented at the Advantage NZ: Geotechnical Petroleum Forum.

Sahoo, T. R., Kroeger, K. F., Thrasher, G., Munday, S., Mingard, H., Cozens, N., Hill, M., 2015. Facies distribution and impact on petroleum migration in the canterbury basin, new zealand.

Sangree, J., Widmier, J., 1977. Seismic stratigraphy and global changes of sea level: Part 9. seismic interpretation of clastic depositional facies: Section 2. application of seismic reflection configuration to stratigraphic interpretation.

Sawyer, D. E., Flemings, P. B., Nikolinakou, M., 2014. Continuous deep-seated slope failure recycles sediments and limits levee height in submarine channels. Geology 42 (1), 15–18.

Schlumberger, 2017. Petrel. Geophysics Help Center (Version 2017.5): Schlumberger.

Shanmugam, G., Moiola, R., 02 1988. Submarine fans: Characteristics, models, classification, and reservoir potential. Earth-Science Reviews Earth-Science Reviews, 383–428.

Shepard, F., Marshall, N., McLoughlin, P., 1974. Currents in submarine canyons. In: Deep sea research and oceanographic abstracts. Vol. 21. Elsevier, pp. 691–706.

Shepard, F. P., 1965. Types of submarine valleys. AAPG Bulletin 49 (3), 304–310.

Shepard, F. P., 1981. Submarine canyons: multiple causes and long-time persistence. AAPG Bulletin 65 (6), 1062–1077.

Shepard, F. P., Marshall, N. F., 1973. Currents along floors of submarine canyons. AAPG Bulletin 57 (2), 244–264.

Sheriff, R. E., Geldart, L. P., 1995. Exploration seismology. Cambridge university press.

Simm, R., Bacon, M., Bacon, M., 2014. Seismic Amplitude: An interpreter's handbook. Cambridge University Press.

Sprague, A., Garfield, T., Goulding, F., Beaubouef, R., Sullivan, M., Rossen, C., Campion, K., Sickafoose, D., Abreu, V., Schellpeper, M., et al., 2005. Integrated slope channel depositional models: the key to successful prediction of reservoir presence and quality in offshore west africa. CIPM, cuarto E-Exitep, 1e13.

Stelting, C. E., Leg, D., Scientists, S., 1985. Migratory characteristics of a mid-fan meander belt, mississippi fan. In: Submarine fans and related turbidite systems. Springer, pp. 283–290.

Stevenson, C. J., Talling, P. J., Wynn, R. B., Masson, D. G., Hunt, J. E., Frenz, M., Akhmetzhanhov, A., Cronin, B. T., 2013. The flows that left no trace: Very large-volume turbidity currents that bypassed sediment through submarine channels without eroding the sea floor. Marine and Petroleum Geology 41, 186–205.

Stirling, M., Pettinga, J., Berryman, K., Yetton, M., 2001. Probabilistic seismic hazard assessment of the canterbury region, new zealand.

Stow, D. A., Mayall, M., 2000. Deep-water sedimentary systems: new models for the 21st century. Marine and Petroleum Geology 17 (2), 125–135.

Straub, K. M., Mohrig, D., Pirmez, C., Prather, B., Deptuck, M., Mohrig, D., vanHoorn, B., Wynn, R., 2012. Architecture of an aggradational tributary submarine channel network on the continental slope offshore brunei darussalam. Application of the principles of seismic geomorphology to continental-slope and base-of-slope systems: case studies from seafloor and near-seafloor analogues. Soc. Sedimentary Geol. Spec. Publ 99, 13–30.

Subrahmanyam, D., Rao, P., 2008. Seismic attributes–a review. In: 7th International Conference & Exposition on Petroleum Geophysics, Hyderabad. pp. 398–404.

Sutherland, R., 1995. The australia-pacific boundary and cenozoic plate motions in the sw pacific: Some constraints from geosat data. Tectonics 14 (4), 819–831.

Sutherland, R., Browne, G., 2003. Canterbury basin offers potential on south island, new zealand. Oil & gas journal 101 (5), 45–49.

Thigpen, B. B., Dalby, A., Landrum, R., 1975. Special report of the subcommittee on polarity standards. Geophysics 40 (4), 694–699.

Thomas, M., Bodin, S., 2013. Architecture and evolution of the finale channel system, the numidian flysch formation of sicily; insights from a hierarchical approach. Marine and Petroleum Geology 41, 163–185.

Todd, B. S., 1984. Interpretation and prospectivity of ppl 38203 canterbury basin, new zealand. New Zealand unpublished openfile petroleum report 1046.

Trewick, S. A., Paterson, A. M., Campbell, H. J., 2007. Guest editorial: hello new zealand. Journal of Biogeography 34 (1), 1–6.

Uruski, C. I., 2010. New zealands deepwater frontier. Marine and Petroleum Geology 27 (9), 2005–2026.

Vail, P. R., 1987. Seismic stratigraphy interpretation using sequence stratigraphy: Part 1: Seismic stratigraphy interpretation procedure.

Veeken, P. C., 2007. 2.5 seismic display.
URL https://app.knovel.com/hotlink/khtml/id:kt007YHVH1/handbook-geophysical/seismic-display

Verney, P., Rainaud, J., Perrin, M., Thonnat, M., 2008. A knowledgebased approach of seismic interpretation: Horizon and dipfault detection by means of cognitive vision. pp. 874–878.
URL https://library.seg.org/doi/abs/10.1190/1.3063780

Walcott, R., 1979. Plate motion and shear strain rates in the vicinity of the southern alps. The origin of the Southern Alps 18, 5–12.

Wallis, G. P., Trewick, S. A., 2009. New zealand phylogeography: evolution on a small continent. Molecular Ecology 18 (17), 3548–3580.

Weimer, P., 1991. Seismic Facies, Characteristics, and Variations in Channel Evolution, Mississippi Fan (Plio-Pleistocene), Gulf of Mexico. Springer New York, New York, NY, pp. 323–347.
URL https://doi.org/10.1007/978-1-4684-8276-8_18

Wells, M., Cossu, R., 2013. The possible role of coriolis forces in structuring large-scale sinuous patterns of submarine channel–levee systems. Philosophical Transactions of the Royal Society A: Mathematical, Physical and Engineering Sciences 371 (2004), 20120366.

White, R., Simm, R., 2003. Tutorial: Good practice in well ties. First Break 21 (10).

Wrona, T., Magee, C., Jackson, C. A., Huuse, M., Taylor, K. G., 2017. Kinematics of polygonal fault systems: observations from the northern north sea. Frontiers in Earth Science 5, 101.

Wynn, R. B., Cronin, B. T., Peakall, J., 2007. Sinuous deep-water channels: Genesis, geometry and architecture. Marine and Petroleum Geology 24 (6-9), 341–387.

Xiujian, D., Guangdi, L., Mingliang, S., Pangen, W., 2013. Origin of polygonal fault systems: A case from the sanzhao sag in the songliao basin, east china. Petroleum Exploration and Development 40 (3), 333–343.

Zeng, H., 2006. Stratal slicing makes seismic imaging of depositional systems easier.

Zeng, H., 2010. Stratal slicing: Benefits and challenges. The Leading Edge 29 (9), 1040–1047.

Zeng, H., Backus, M. M., Barrow, K. T., Tyler, N., 1998. Stratal slicing, part i: realistic 3-d seismic model. Geophysics 63 (2), 502–513.

Zeng, H., John, A., Jackson, K. G., Dommisse, R., 2011. Stratal slice: a tool for seismic sedimentologic imaging and reservoir prediction. In: 12th International Congress of the Brazilian Geophysical Society.

Zhao, T., Zhang, J., Li, F., Marfurt, K. J., 2016. Characterizing a turbidite system in canterbury basin, new zealand, using seismic attributes and distance-preserving self-organizing maps. Interpretation 4 (1), SB79–SB89.

Appendix A: Polygonal Faults System in the Study area

The polygonal fault system generally occurs within fine-grained sedimentary successions, that mostly acts as a seal for the reservoirs (Wrona et al., 2017). Waka 3D seismic survey reveals the presence of extensive Paleocene and Eocene polygonal fault system and these extensive layer bound normal fault systems typically develop in fine-grained sediments during the early stage of burial compaction (Sahoo et al., 2014). The detailed geometry of polygonal faults is shown in (Figure:7.1) interpreted in Waka 3D seismic survey.
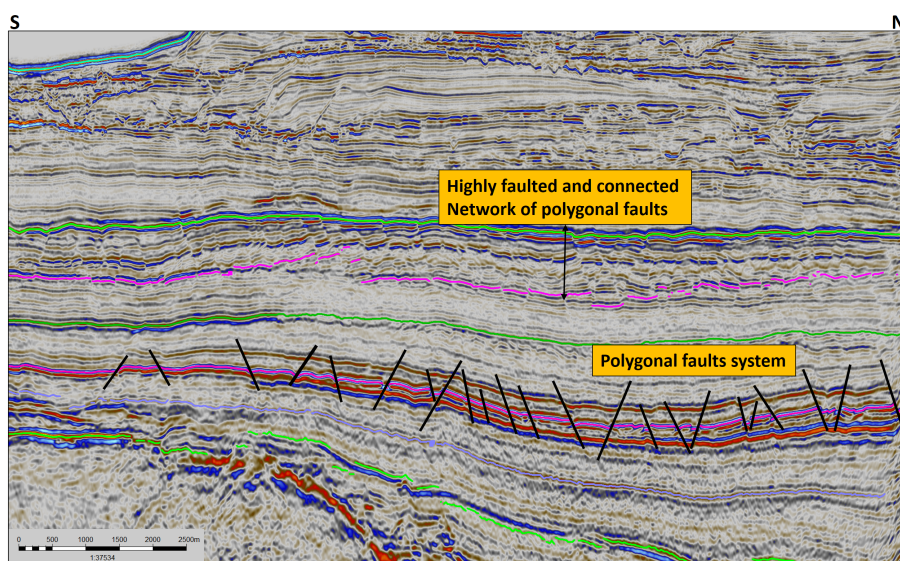
Figure 1: Polygonal faults system Waka 3D Seismic reflection survey.

Variance attribute is used to extract the polygonal fault system in Waka 3d seismic survey. Variance attribute, which is an edge method measures the similarity of wave-forms or traces adjacent over given lateral and/or vertical windows (Koson et al., 2014). The variance attribute isolates discontinuities in the horizontal continuity of amplitude from the Waka 3D seismic survey. However, the variance is good to work in a short window it helps to bring out the depositional features on the other hand dip guided variance is useful for extracting structural features like faults (Schlumberger, 2017). The extracted variance attribute from Waka 3D seismic survey (Figure:7.2) shows polygonal fault system presence at Paleocene and Eocene level which are correlated with the seismic signature of polygonal faults system at the same location (Figure:7.1).
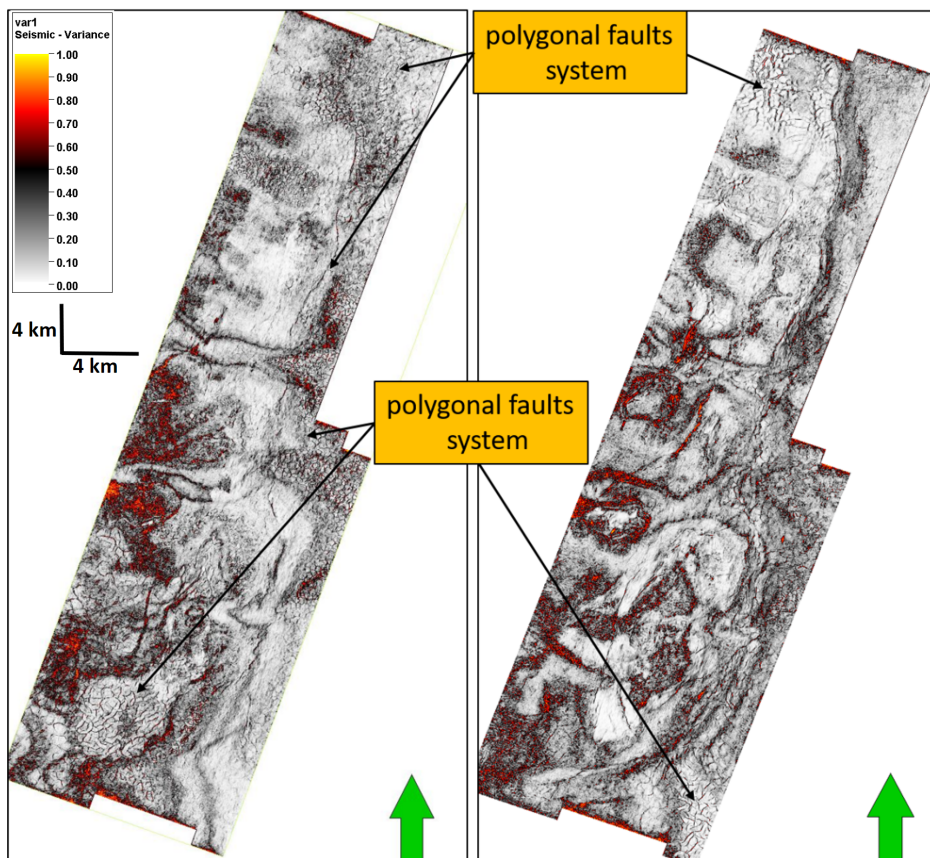
Figure 2: Polygonal fault system shown on variance attribute.

Appendix B: Morphometric data for different authors for comparisons

Gambo et al. (2012)		Harishidayat et al. (2018)			Qin et al. (2011)				
Dist(m)	Ht(m)	Dist(m)	Width (m)	Dist(m)	Height (m)	Dist(m)	Width(m)	Dist(m)	Height (m)	Width (m)
0	170	0	410	0	150	0	200	625	153.92	830
700	151	1300	500	1500	280	1500	400	750	147.26	792
1700	137	1800	450	3000	150	4000	500	875	136.16	782
2000	180	2800	650	5000	300	6500	150	4250	118.4	681
2200	158	4200	590	7000	160	8000	800	4375	114.7	698
3000	175	5000	760	8000	280	11000	1100	4500	114.7	740
3900	143	5800	430	8300	180	12000	500	4625	118.4	774
4200	175	6400	680	9000	370			4750	108.78	709
4700	120	7000	520	11000	250			7500	151.7	923
5800	160	8200	780	11700	300			7625	150.22	876
6600	138	9600	820	11900	200			7750	143.56	957
7200	150	11000	400	12000	280			7875	139.86	977
7800	102	11600	580					8000	131.72	895
9000	140	12600	380					8125	133.94	907
9800	100	15000	600					8250	134.68	1061
10000	138	17200	420					8375	137.64	1027
11800	88	19000	780					8500	141.34	1026
12400	110	19800	620					8625	145.78	1052
13000	100							20625	19.98	455
13800	132							24250	35.52	333
14000	158							31375	91.02	623
15400	140							41500	33.3	482
16200	164							41625	30.34	487
17000	158							41750	28.86	497
17400	180							41875	28.12	504
18200	160							42000	27.38	477
19000	180							42125	26.64	461
20000	162							42250	25.9	445

Table: Morphometric data for different authors for comparisons

Appendix C: Morphometric data for eighteen channels & cross-plots in the Waka 3D survey

	Height (m)				Gradient				Sinuosity				Aspect ratio (width/height)		
	Max	Min	Average		Max	Min	Average		Max	Min	Average		Max	Min	Average
Channels															
1	308	151	230		1.77	0.71	1.14		1.56	1.02	1.18		11.1	5.67	8.19
1a	286	215	251		1.64	1.16	1.41		1.19	1.04	1.12		12.0	8.56	10.25
1b	220	160	190		1.05	0.76	0.86		0.99	0.91	0.97		16.5	9.90	13.96
2	237	150	201		1.08	0.58	0.86		2.00	1.03	1.11		32.9	19.44	24.00
3	450	272	361		3.00	1.81	2.39		0.91	0.64	0.85		9.5	6.34	7.86
3a	386	305	346		2.55	1.67	2.07		1.32	1.01	1.13		12.2	9.46	10.65
3b	405	294	350		2.30	1.40	1.72		1.07	0.88	1.00		12.9	8.29	10.05
4	380	207	294		1.73	0.65	1.17		1.06	0.64	0.87		14.1	9.07	11.63
5	214	145	180		1.47	0.91	1.18		1.11	0.99	1.05		8.0	5.37	6.92
6	242	208	225		1.61	1.39	1.53		1.38	1.04	1.13		9.9	7.48	8.58
7	190	135	163		1.05	0.62	0.90		1.52	1.03	1.14		22.4	11.73	15.62
8	340	295	318		1.78	1.24	1.48		1.11	0.98	1.06		8.8	6.61	7.78
9	320	107	214		2.13	0.71	1.31		1.95	0.88	1.06		39.4	16.00	24.44
10	263	201	232		1.28	0.72	0.97		1.03	0.86	0.98		9.4	7.48	8.29
11	353	285	319		2.08	1.40	1.71		1.08	0.95	1.03		11.3	6.77	8.97
12	320	290	305		1.75	1.08	1.31		1.09	0.42	0.95		12.9	8.91	11.00
13	410	272	341		2.36	1.42	1.79		1.03	0.98	1.00		11.7	7.85	9.52
14	196	167	182		1.05	0.76	0.87		1.04	0.70	0.93		10.4	6.97	8.10

|	CSA (km2)				Base width				Top width				Width ratio average		
	Max	Min	Average		Max	Min	Average		Max	Min	Average		Top	base	Ratio
Channels															
1	0.05	0.01	0.03		577	135	343		2564	973	1805		1805	343	0.19
1a	0.09	0.05	0.08		595	204	400		2877	1944	2563		2563	400	0.16
1b	0.10	0.05	0.07		553	205	348		3066	1644	2531		2531	348	0.14
2	0.12	0.07	0.10		910	535	704		5838	4490	4788		4788	704	0.15
3	0.05	0.03	0.04		896	353	585		3359	2443	2798		2798	585	0.21
3a	0.09	0.06	0.07		624	400	531		4340	3360	3810		3810	531	0.14
3b	0.10	0.05	0.08		590	195	357		3980	2919	3470		3470	357	0.10
4	0.12	0.03	0.07		850	260	405		5068	2195	3582		3582	405	0.11
5	0.09	0.03	0.07		280	160	229		1546	778	1291		1291	229	0.18
6	0.07	0.05	0.06		395	234	328		2257	1690	1963		1963	328	0.17
7	0.08	0.03	0.06		450	180	269		3130	2147	2670		2670	269	0.10
8	0.09	0.06	0.08		500	285	369		2645	1995	2400		2400	369	0.15
9	0.12	0.01	0.05		930	407	650		6763	2040	4664		4664	650	0.14
10	0.04	0.03	0.03		445	215	327		2237	1790	1976		1976	327	0.17
11	0.12	0.01	0.06		630	220	384		3908	2012	3061		3061	384	0.13
12	0.08	0.05	0.07		515	330	436		3821	2612	3285		3285	436	0.13
13	0.05	0.03	0.04		630	360	474		3520	2780	3252		3252	474	0.15
14	0.08	0.06	0.07		278	185	227		1798	1304	1483		1483	227	0.15

Table: Morphometric data for eighteen channels in the Waka 3D survey
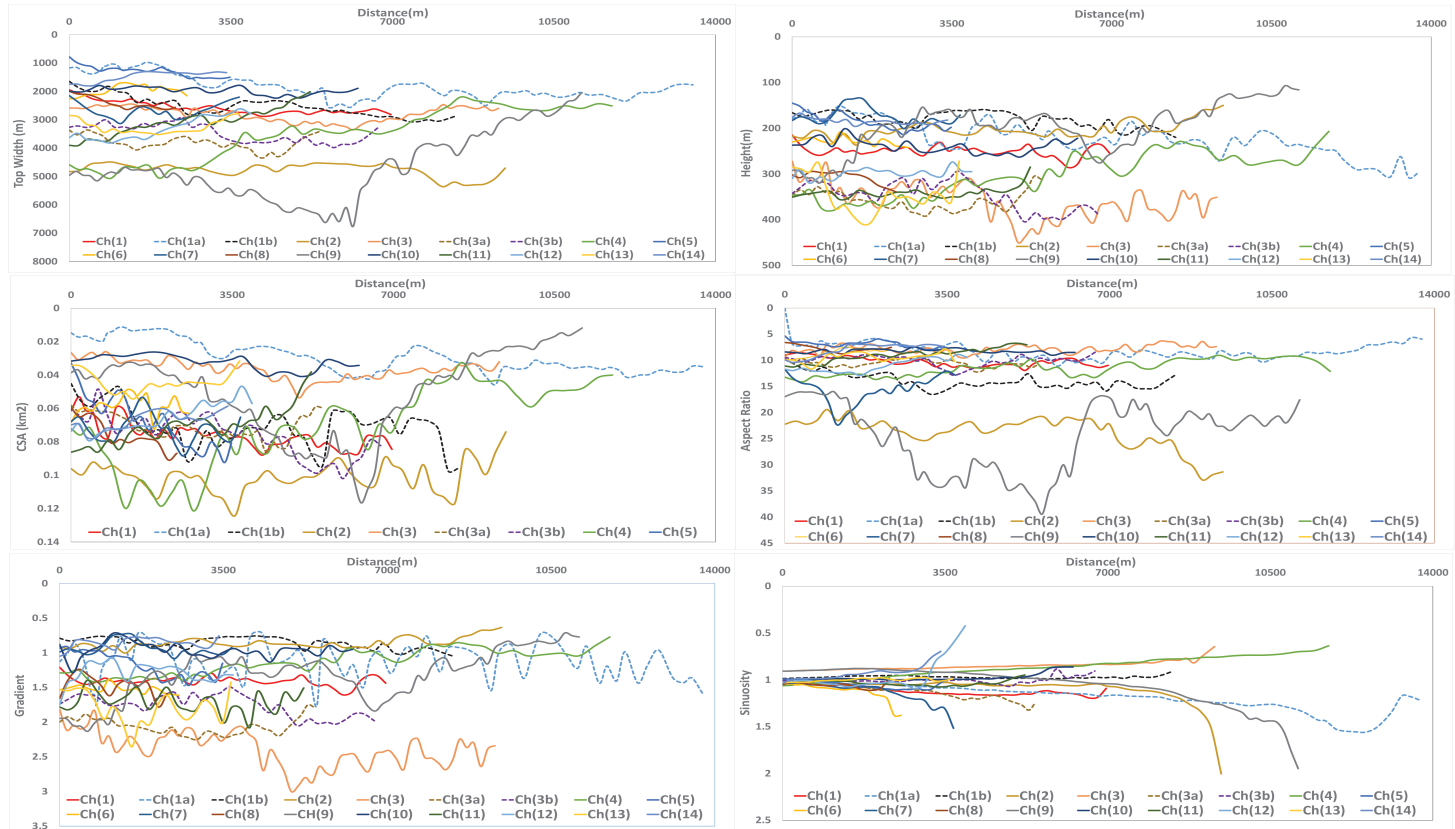
Figure: Cross-plots for eighteen channels in the Waka 3D survey.